Contrib Mineral Petrol (2003) 146: 100–119
DOI 10.1007/s00410-003-0486-6

ORIGINAL PAPER

**Antonio Acosta-Vigil · David London**
**George B. Morgan VI · Thomas A. Dewers**

# Solubility of excess alumina in hydrous granitic melts in equilibrium with peraluminous minerals at 700–800 °C and 200 MPa, and applications of the aluminum saturation index

Received: 12 May 2002 / Accepted: 20 April 2003 / Published online: 12 July 2003


**Abstract** We have studied the controls on the Aluminum Saturation Index (ASI = molec. $Al_2O_3/[(CaO)+(Na_2O)+(K_2O)]$) and the concentration of normative corundum of granitic liquids saturated in alumina by equilibrating peraluminous minerals with initially metaluminous haplogranitic minimum composition liquids at 700–800 °C and 200 MPa, at, and below $H_2O$ saturation. The ASI and normative corundum increase with increasing $H_2O$ concentration in the melt (≈0.04 to 0.10 moles excess $Al_2O_3$ per mole of $H_2O$), temperature, and with addition of the non-haplogranitic components Fe, Mg, and B. The ASI parameter and concentration of normative corundum cannot be used to monitor $aAl_2O_3$ between different mineral assemblages and melt because other components that affect the solubility of alumina, including $H_2O$, Fe, Mg, and B, do not appear in their formulations. ASI and normative corundum, however, provide petrogenetic information about magmas generated by partial melting of strongly peraluminous protoliths by virtue of their regular and predictable variation with melt composition (e.g., $H_2O$ concentration) and temperature. For the application of these data to natural rocks it is necessary to choose as an analogue system the ASI-solubility or normative corundum-solubility relations of the most chemically complex peraluminous mineral present in the rock. Comparison of ASI values of anatectic leucosomes and allochthonous leucogranites with experimentally predicted values suggests low $H_2O$ concentrations in melt during crustal partial melting. Rapid melt segregation before equilibration with restitic peraluminous phases is also suggested in some cases.

A. Acosta-Vigil (✉) · D. London · G. B. Morgan VI
T. A. Dewers
School of Geology and Geophysics, University of Oklahoma,
100 East Boyd Street, Room 810 SEC, Norman,
OK 73019, USA
E-mail: aacosta@hoth.gcn.ou.edu
Tel.: +1-405-3253253
Fax: +1-405-3253140

Editorial responsibility: I. Carmichael

## Introduction

The molar ratio $Al_2O_3/[(CaO)+(Na_2O)+(K_2O)]$, referred to as the Aluminum Saturation Index or ASIby Zen (1986), is a well-known compositional parameter used in igneous petrology for characterizing rocks and deriving petrogenetic interpretations. For instance, a distinctive feature of crustal granites derived by the anatexis of metasediments (S-type) is an ASI≥1.05–1.10 and typically between 1.10 and 1.30 (Chappell and White 1974; White and Chappell 1977; Chappell 1999). The work presented here focuses on crustally derived granites, and how the ASI values are established in liquids derived from peraluminous sources.

The ASI of granitic melts derived by partial melting of peraluminous rocks will depend on the saturation values of peraluminous minerals in melt, as well as the interplay between the kinetics of peraluminous mineral dissolution and the time interval between magma generation and the separation of melt from the restite. Despite several previous studies concerning the effect of excess aluminum on phase equilibria in granitic melts (e.g., Holtz et al 1992a, 1992b; Joyce and Voight 1994), the ASI of granitic melts in equilibrium with different peraluminous phases is not well defined by natural occurrences or by experiments. Acosta-Vigil et al. (2002) examined the kinetics of equilibration between corundum or andalusite and $H_2O$-saturated metaluminous haplogranitic melts. They concluded that diffusion is sufficiently rapid, except perhaps in magmas with low $H_2O$ concentrations, that equilibrium usually should be attained between restitic corundum or andalusite and melt in the likely time frame in which melt and restite remain in contact (e.g., Copeland et al. 1990; Watt et al. 1996; Ayres et al. 1997; see also Sawyer 1991; Barbero et al. 1995; Harris et al. 2000). This paper complements Acosta-Vigil et al. (2002) by assessing the ASI value of melts in equilibrium with different peraluminous minerals at, and below, $H_2O$ saturation of melt at 700–800 °C and 200 MPa.

The experiments reported here are designed to equilibrate $H_2O$-saturated and $H_2O$-undersaturated haplogranitic liquids with one each of a suite of important peraluminous phases at 700–800 °C and 200 MPa. The experimental design is one in which crystal-free pools of melt react with large quantities of disseminated mineral grains such that diffusion distances are minimized, permitting crystal-liquid equilibrium to be approached over short experimental time frames. The method also facilitates accurate electron microprobe analysis of the glasses, which is a nontrivial problem for hydrous alkali aluminosilicate glasses (Morgan and London 1996).

## Materials and methods

### Starting materials and experimental methods

The starting material for granitic liquid was a synthetic anhydrous glass (Corning Lab Services, New York) with the nominal composition of the $H_2O$-saturated metaluminous haplogranite minimum at 200 MPa (Tuttle and Bowen 1958). Sources of excess aluminum included natural, gem-quality crystals of corundum (source unknown), andalusite (Minas Gerais, Brazil), kyanite (Minas Gerais, Brazil), and cordierite (India), as well as natural tourmaline (Little Three pegmatite, California), sillimanite (Peña Negra migmatites, central Spain, Pereira and Bea 1994), muscovite (Minas Gerais, Brazil), and boehmite powder (prepared by dehydrating reagent-grade synthetic gibbsite at 400 °C in air, grain size $< 50$ μm). Table 1 shows the composition of starting glass and peraluminous crystalline phases determined by electron microprobe.

The haplogranitic glass and peraluminous minerals were ground separately in an agate mortar under ethanol, and the fraction with grain size between 0.1 and 1 mm was collected and oven dried. Separate mixtures of glass and a single peraluminous phase were prepared in weight proportions in the range of 1:3 to 1:1, and homogenized by tumbling for 24 h. Mineral-glass mixtures and variable amounts of deionized and ultra-filtered water were loaded into gold or platinum capsules (3 mm ID). The capsules were sealed by arc welding while keeping the lower end of the capsule cold to prevent volatilization of added water. The capsules were weighed before and after welding, and then again after overnight heating at 120 °C to ensure no water loss. Experiments were conducted in NIMONIC 105 cold-seal pressure vessels inclined ≈15° from horizontal. The vessels were first pressurized at 200 MPa, and then heated to the run conditions between 700 and 800 °C for durations ranging from 240 to 4,320 h. Pressure was measured with a factory-calibrated Heise Bourdon tube gauge, and temperature was monitored with internal Chromel-Alumel thermocouples. Uncertainties in pressure and temperature are $< 10$ MPa and $\pm 4$ °C, respectively. Variations from targeted conditions during the experiment were less than 10 bars and 2 °C. Oxygen fugacity, calibrated with respect to the solubility of cassiterite in $H_2O$-saturated haplogranite liquid (Taylor and Wall 1992; Linnen et al. 1995), is indirectly controlled by the composition of the vessels at ≈0.5 log units below the Ni-NiO buffer in the temperature range of these experiments. Experiments were quenched at a rate of ≈75 °C/min using a jet of air and water. After quenching, the capsules were weighed to check for leakage and punctured to check for the presence of free

**Table 1** Electron microprobe analyses (wt%) of starting materials

| Material | Anhydrous starting glass | $H_2O$-saturated starting glass | Corundum | Sillimanite | Andalusite | Kyanite | Cordierite | Muscovite | Tourmaline |
|---|---|---|---|---|---|---|---|---|---|
| No. analyses | 29 | 10 | 15 | 15 | 40 | 10 | 15 | 10 | 22 |
| $SiO_2$ | 77.69 (0.51) | 73.58 (0.45) | 0.03 (0.02) | 35.88 (0.41) | 36.32 (0.20) | 37.09 (0.17) | 47.93 (0.31) | 45.16 (0.38) | 36.78 (0.75) |
| $TiO_2$ | 0.01 (0.01) | 0.01 (0.01) | 0.01 (0.01) | 0.02 (0.02) | 0.04 (0.02) | 0.01 (0.01) | 0.02 (0.01) | 0.12 (0.02) | 0.10 (0.05) |
| $Al_2O_3$ | 13.02 (0.16) | 11.74 (0.17) | 99.47 (0.91) | 62.80 (1.13) | 64.02 (0.35) | 62.99 (0.24) | 33.05 (0.55) | 35.38 (0.38) | 36.19 (0.89) |
| FeO[a] | 0.02 (0.01) | 0.02 (0.01) | 0.85 (0.03) | 0.17 (0.02) | 0.31 (0.12) | 0.19 (0.03) | 8.11 (0.19) | 1.85 (0.03) | 8.97 (0.33) |
| MnO | 0.00 (0.00) | 0.01 (0.01) | 0.01 (0.01) | 0.01 (0.01) | 0.00 (0.01) | 0.00 (0.01) | 0.28 (0.04) | 0.05 (0.01) | 1.55 (0.90) |
| MgO | 0.01 (0.00) | 0.01 (0.00) | 0.01 (0.00) | 0.01 (0.01) | 0.09 (0.05) | 0.03 (0.01) | 8.67 (0.13) | 0.29 (0.01) | 2.13 (1.32) |
| ZnO | n.d. | n.d. | 0.01 (0.01) | 0.02 (0.02) | 0.00 (0.01) | 0.01 (0.01) | 0.02 (0.02) | 0.02 (0.01) | 0.22 (0.30) |
| CaO | 0.01 (0.01) | 0.13 (0.10) | 0.01 (0.01) | 0.01 (0.01) | 0.00 (0.00) | 0.01 (0.00) | 0.02 (0.02) | 0.00 (0.00) | 0.11 (0.08) |
| BaO | 0.01 (0.01) | 0.01 (0.02) | 0.01 (0.02) | 0.01 (0.02) | n.d. | 0.01 (0.02) | 0.01 (0.02) | 0.01 (0.02) | 0.01 (0.01) |
| $Na_2O$ | 4.60 (0.11) | 4.26 (0.12) | 0.02 (0.04) | 0.06 (0.07) | 0.01 (0.01) | 0.00 (0.00) | 0.25 (0.10) | 0.78 (0.03) | 1.37 (0.13) |
| $K_2O$ | 4.78 (0.09) | 4.64 (0.12) | 0.00 (0.00) | 0.01 (0.01) | 0.00 (0.00) | 0.00 (0.00) | 0.03 (0.02) | 9.96 (0.11) | 0.02 (0.01) |
| $P_2O_5$ | n.d. | 0.04 (0.02) | n.d. | n.d. | n.d. | n.d. | n.d. | n.d. | n.d. |
| $B_2O_3$ | n.d. | n.d. | n.d. | n.d. | n.d. | n.d. | n.d. | n.d. | n.d. |
| F | 0.03 | 0.01 (0.02) | 0.02 (0.03) | 0.03 (0.04) | n.d. | 0.02 (0.03) | 0.02 (0.04) | 0.49 (0.10) | 0.16 (0.13) |
| Cl | 0.01 | 0.01 (0.01) | 0.01 (0.00) | 0.00 (0.00) | n.d. | 0.00 (0.00) | 0.00 (0.01) | 0.01 (0.00) | 0.00 (0.00) |
| O = F | −0.01 | −0.01 | −0.01 | −0.01 | | | −0.01 | −0.21 | −0.07 |
| O = Cl | | | 0.00 | 0.00 | | | 0.00 | 0.00 | 0.00 |
| Total | 100.18 | 94.46 | 100.43 | 98.99 | | 100.36 | 98.39 | 93.90 | 87.54 |
| $H_2O$ EMPA-diff | | 5.54 | | | | | | | |
| Moles Mg/Mg + Fe | | | | | | | 0.66 | 0.22 | 0.30 |
| ASI | 1.020 | 0.956 | | | | | | | |

[a]Total Fe expressed as FeO

water. After drying, the capsules were weighed again, and charges were mounted in epoxy and polished for microprobe analysis.

All the experiments were conducted in the forward-direction, in the sense that mixtures of haplogranitic glass, $H_2O$ (amounts controlled to yield melts at and below $H_2O$ saturation at experimental temperature and pressure), and a single peraluminous phase (corundum, boehmite, sillimanite, andalusite, kyanite, muscovite, cordierite, tourmaline) were heated directly to 700 °C, 750 °C or 800 °C. Table 2 lists the starting materials and conditions in all the experiments, as well as some compositional properties of the resultant glasses.

## Analytical methods

The starting anhydrous glass, peraluminous crystalline phases and experimental glasses were analyzed with a Cameca SX-50 electron microprobe at the University of Oklahoma. Matrix reduction used the PAP correction algorithm (Pouchou and Pichoir 1985). During electron microprobe analysis (EMPA), hydrous alkali aluminosilicate glasses are especially susceptible to alkali migration or volatilization and concomitant changes in major elemental ratios. To achieve high accuracy, glasses were analyzed using two beam conditions as described by Morgan and London (1996). An initial condition of 20 kV acceleration, 2 nA beam current, and 20 μm defocused spot was used for sodium, potassium, aluminum and silicon (sodium and aluminum were analyzed first and concurrently). Counting times were 30 s on peak for all elements, yielding calculated 3-$\sigma$ minimum detection limits of $\leq 0.02$ wt% for $Na_2O$, $K_2O$ and $Al_2O_3$, and $\approx 0.05$ wt% for $SiO_2$. Uncertainties based on counting statistics are in the range of 0.5–1.0% of the reported concentrations for $SiO_2$ and $Al_2O_3$, and 1.5–3.0% for $Na_2O$ and $K_2O$. Table 3 illustrates the importance of conducting the proper EMPA procedure by comparing the composition of a hydrous experimental glass (used as a standard in the EMP laboratory at the University of Oklahoma) to EMPA results obtained with three different beam conditions. The conditions recommended by Morgan and London (1996) yield a good fit to the composition reported for the standard, but analyses with smaller spot sizes and higher beam currents produce very substantial loss of sodium and grow-in (progressive increase) in aluminum. As a consequence, the errors associated with the ASI values can be enormous, rendering the analyses useless regarding this parameter if improper beam conditions are used. For granitic glasses, Morgan and London (1996) also determined that corrections based on anhydrous glasses as standards are invalid. Higher-energy focused beams and corrections based on anhydrous glass standards have been widely used in most previous studies of a similar nature; in such cases, the values of ASI and major alkali aluminosilicate components are incorrect to varying degrees. In our analyses, the maximum uncertainty for reported ASI values is $\pm 0.035$, calculated by the propagation of errors. The elements Ti, Fe, Mg, Mn, P, Ba, F, and Cl in boron-absent glasses were subsequently analyzed using a 20-kV, 2-nA, 20-μm beam, and counting times of 30 s. The same elements in boron-added compositions were analyzed with a 15-kV, 40-nA, 20-μm beam; counting times were 20 s for all elements except B and Mg, which were counted for 30 s. In each experiment, 10 to 35 spot analyses of glass were acquired within ≈30–50 μm of the mineral grains. In addition, analytical transverses across melt pools ≈200–400 μm in diameter were acquired to examine homogeneity as an indicator of bulk mineral-melt equilibrium.

Accurate values for all components, including $H_2O$, were necessary for the successful interpretation of the experimental results. $H_2O$ concentrations of glass were assessed primarily by difference of the EMPA totals from 100%. Previous investigations (Morgan and London 1996) have shown that this technique provides acceptable accuracy using the EMP analytical methods described above. This result was tested again in the current study by analysis of hydrous albite glasses with 2 to 10 wt% $H_2O$, provided by Silver and Stolper (same glasses used in their calibration of $H_2O$ analysis by Fourier transform infrared (FTIR) spectroscopy, Silver and Stolper 1989). Additionally, these results were tested by comparison of our analytical results for selected samples with direct analysis of hydrogen by secondary ion mass spectroscopy (SIMS) using a Cameca 3f ion microprobe (Richard Hervig, Arizona State University). Standards for SIMS analyses were hydrous rhyolitic glasses for which $H_2O$ contents were determined by Karl Fischer titration (KFT). Hydrogen counts were converted to $H_2O$ concentrations by reference to $SiO_2$ contents determined by electron microprobe. Finally, reproducibility of $H_2O$ determination by EMPA difference was evaluated by replicate analysis of selected samples over more than one analytical session.

Comparison of the results of $H_2O$ concentrations by EMPA difference and by direct analysis with SIMS or FTIR spectroscopy is shown in Table 4. We obtained a good match between reported $H_2O$ contents of the hydrous albite glasses (Silver and Stolper 1989) and those obtained by the EMPA method. Results by EMPA and SIMS agree reasonably well (0 to 18% relative difference, mean ≈9%) for glasses with low $H_2O$ concentrations. At high $H_2O$ contents, however, the SIMS method yields systematically ≈9% to 45% (mean ≈30%) lower relative values. Replicate analyses on six of our experimental glasses by EMPA shows that the results are reproducible in different analytical sessions to within ≈9% relative.

Estimation of $H_2O$ by EMPA difference indicates 5.5–6.5 wt% $H_2O$ in our starting metaluminous glass hydrated at 200 MPa and 800 °C, which compares well with values of 5.8–6.3 wt% $H_2O$ reported by Holtz et al. (1992c, 1995) and Behrens and Jantos (2001) using KFT analysis on similar $H_2O$-saturated glasses and conditions (Table 4). Pending a more exhaustive study, we suggest that the deviation between EMPA and SIMS analyses at high $H_2O$ concentration is a characteristic of the SIMS calibration or ion yield. From our comparison of the EMPA values with FTIR (albite glasses) and KFT (glasses at the haplogranite minimum), we conclude that $H_2O$ concentrations assessed by EMPA difference, using the current analytical methods, are reliable and accurate to within $\pm 10\%$ relative.

## Results

### Run products

$H_2O$-undersaturated experiments (800 °C) always involved nucleation and growth of new crystalline material at the mineral-melt interfaces, consisting either of scarce ternary feldspar crystals (Fig. 1a) or abundant feldspar-quartz integrowths (Fig. 1b). Tourmaline dissolution experiments also produced euhedral corundum, aluminosilicate, cordierite and spinel close to the interfaces (Fig. 1c), whereas dissolution of sillimanite produced mainly euhedral cordierite plus some magnetite overgrown by hercynitic spinel. Magnetite was the only phase that crystallized in cordierite dissolution experiments.

$H_2O$-saturated experiments at 700 °C involved dissolution of the peraluminous mineral phases and crystallization of alkali feldspar at or close to the mineral-glass interfaces (Fig. 1d). Tourmaline dissolution experiments also produced euhedral corundum close to the interfaces. $H_2O$-saturated experiments at 750 °C and 800 °C were dominated by dissolution of the peraluminous minerals in the case of andalusite and cordierite (Fig. 1e). Starting boehmite (Fig. 1f) was transformed to aggregates of euhedral corundum plates (Fig. 1g). The dissolution of kyanite was accompanied by crystallization

**Table 2** Starting materials, temperature, duration, and some chemical features of the product glasses of all the conducted mineral dissolution experiments

| Run no. | Starting materials | $H_2O$[a] (wt%) | Temperature (°C) | Duration (h) | Melt ASI (SD) | Normative corundum | Mole fraction of $Al_2O_3$ | $B_2O_3$ wt% (SD) | $H_2O$[b] (wt%) | No. analyses |
|---|---|---|---|---|---|---|---|---|---|---|
| Acasi 45 | $H_2O$ + 75 wt% Corundum + 25 wt% haplogranite glass | 32.55 | 700 | 480 | 1.152 (0.043) | 1.95 | 0.0711 | n.d. | 7.36 | 15 |
| Acasi 38 | $H_2O$ + 75 wt% Corundum + 25 wt% haplogranite glass | 38.40 | 700 | 2160 | 1.187 (0.041) | 2.16 | 0.0700 | n.d. | 7.76 | 10 |
| Acasi 113 | $H_2O$ + 75 wt% Corundum + 25 wt% haplogranite glass | 15.82 | 700 | 4320 | 1.175 (0.031) | 1.92 | 0.0692 | n.d. | 7.27 | 15 |
| Acasi 240 | $H_2O$ + 75 wt% Corundum + 25 wt% haplogranite glass | 15.62 | 750 | 2184 | 1.165 (0.031) | 1.87 | 0.0725 | n.d. | 6.13 | 20 |
| Acasi 121 | $H_2O$ + 75 wt% Corundum + 25 wt% haplogranite glass | 3.08 | 800 | 480 | 1.123 (0.030) | 1.43 | 0.0754 | n.d. | 3.48 | 10 |
| Acasi 135 | $H_2O$ + 75 wt% Corundum + 25 wt% haplogranite glass | 3.28 | 800 | 960 | 1.103 (0.033) | 1.15 | 0.0715 | n.d. | 3.54 | 10 |
| Acasi 189 | $H_2O$ + 75 wt% Corundum + 25 wt% haplogranite glass | 2.85 | 800 | 1100 | 1.115 (0.035) | 1.29 | 0.0737 | n.d. | 3.29 | 20 |
| Acasi 54 | $H_2O$ + 75 wt% Corundum + 25 wt% haplogranite glass | 33.49 | 800 | 240 | 1.182 (0.042) | 2.12 | 0.0697 | n.d. | 8.14 | 11 |
| Acasi 44 | $H_2O$ + 75 wt% Corundum + 25 wt% haplogranite glass | 41.44 | 800 | 480 | 1.167 (0.033) | 2.05 | 0.0726 | n.d. | 6.94 | 15 |
| Acasi 49 | $H_2O$ + 75 wt% Corundum + 25 wt% haplogranite glass | 3.43 | 800 | 480 | 1.181 (0.022) | 2.41 | 0.0979 | n.d. | 6.81 | 10 |
| Acasi 80 | $H_2O$ + 75 wt% Corundum + 25 wt% haplogranite glass | 19.78 | 800 | 960 | 1.240 (0.055) | 2.64 | 0.0737 | n.d. | 7.08 | 10 |
| Acasi 91 | $H_2O$ + 75 wt% Corundum + 25 wt% haplogranite glass | 2.77 | 800 | 960 | 1.185 (0.024) | 2.22 | 0.0736 | n.d. | 7.21 | 26 |
| Acasi 188 | $H_2O$ + 75 wt% Corundum + 25 wt% haplogranite glass | 10.57 | 800 | 1100 | 1.175 (0.040) | 1.99 | 0.0727 | n.d. | 6.70 | 20 |
| Acasi 96 | $H_2O$ + 10 wt% Boehmite + 90 wt% haplogranite glass | 9.76 | 700 | 240 | 1.094 (0.020) | 0.99 | 0.0656 | n.d. | 6.02 | 13 |
| Acasi 116 | $H_2O$ + 30 wt% Boehmite + 70 wt% haplogranite glass | 9.65 | 700 | 4320 | 1.170 (0.031) | 1.87 | 0.0697 | n.d. | 7.15 | 20 |
| Acasi 145–2 | $H_2O$ + 50 wt% Boehmite + 50 wt% haplogranite glass | 11.11 | 700 | 4320 | 1.162 (0.036) | 2.03 | 0.0737 | n.d. | 7.63 | 19 |
| Acasi 250 | $H_2O$ + 30 wt% Boehmite + 70 wt% haplogranite glass | 10.04 | 750 | 480 | 1.162 (0.029) | 1.83 | 0.0709 | n.d. | 7.19 | 30 |
| Acasi 252 | $H_2O$ + 30 wt% Boehmite + 70 wt% haplogranite glass | 12.09 | 750 | 1392 | 1.187 (0.033) | 2.10 | 0.0721 | n.d. | 7.09 | 20 |
| Acasi 251 | $H_2O$ + 30 wt% Boehmite + 70 wt% haplogranite glass | 8.83 | 750 | 2160 | 1.173 (0.030) | 1.96 | 0.0720 | n.d. | 7.08 | 20 |
| Acasi 94 | $H_2O$ + 10 wt% Boehmite + 90 wt% haplogranite glass | 3.18 | 800 | 240 | 1.096 (0.026) | 1.15 | 0.0734 | n.d. | 3.19 | 12 |
| Acasi 166 | $H_2O$ + 10 wt% Boehmite + 90 wt% haplogranite glass | 2.61 | 800 | 960 | 1.068 (0.033) | 0.78 | 0.0711 | n.d. | 3.3 | 27 |
| Acasi 95 | $H_2O$ + 10 wt% Boehmite + 90 wt% haplogranite glass | 11.47 | 800 | 240 | 1.189 (0.042) | 1.90 | 0.0762 | n.d. | 6.45 | 15 |
| Acasi 134 | $H_2O$ + 10 wt% Boehmite + 90 wt% haplogranite glass | 10.57 | 800 | 960 | 1.171 (0.013) | 2.04 | 0.0763 | n.d. | 6.37 | 10 |
| Acasi 154 | $H_2O$ + 30 wt% Boehmite + 70 wt% haplogranite glass | 12.29 | 800 | 960 | 1.190 (0.023) | 2.15 | 0.0734 | n.d. | 6.54 | 20 |
| Acasi 155 | $H_2O$ + 30 wt% Boehmite + 70 wt% haplogranite glass | 2.83 | 800 | 960 | 1.165 (0.030) | 1.90 | 0.0752 | n.d. | 5.35 | 20 |
| Acasi 144 | $H_2O$ + 50 wt% Boehmite + 50 wt% haplogranite glass | 12.96 | 800 | 480 | 1.199 (0.048) | 2.28 | 0.0755 | n.d. | 6.59 | 10 |
| Acasi 148 | $H_2O$ + 50 wt% Boehmite + 50 wt% haplogranite glass | 2.98 | 800 | 480 | 1.181 (0.029) | 2.09 | 0.0735 | n.d. | 7.22 | 6 |
| Acasi 165 | $H_2O$ + 50 wt% Boehmite + 50 wt% haplogranite glass | 1.79 | 800 | 960 | 1.193 (0.020) | 2.23 | 0.0751 | n.d. | 6.67 | 35 |
| Acasi 167 | $H_2O$ + 50 wt% Boehmite + 50 wt% haplogranite glass | 10.3 | 800 | 960 | 1.181 (0.028) | 2.10 | 0.0749 | n.d. | 6.52 | 25 |
| Acasi 43 | $H_2O$ + 75 wt% Andalusite + 25 wt% haplogranite glass | 50.54 | 700 | 480 | 1.148 (0.031) | 1.79 | 0.0665 | n.d. | 8.95 | 15 |
| Acasi 35 | $H_2O$ + 75 wt% Andalusite + 25 wt% haplogranite glass | 45.38 | 700 | 2160 | 1.145 (0.024) | 1.72 | 0.0683 | n.d. | 7.61 | 10 |
| Acasi 112 | $H_2O$ + 75 wt% Andalusite + 25 wt% haplogranite glass | 19.10 | 700 | 4320 | 1.160 (0.025) | 1.73 | 0.0681 | n.d. | 7.21 | 15 |
| Acasi 244 | $H_2O$ + 75 wt% Andalusite + 25 wt% haplogranite glass | 15.14 | 750 | 480 | 1.161 (0.025) | 1.78 | 0.0693 | n.d. | 6.83 | 30 |
| Acasi 253 | $H_2O$ + 75 wt% Andalusite + 25 wt% haplogranite glass | 15.93 | 750 | 1392 | 1.142 (0.028) | 1.58 | 0.0686 | n.d. | 7.35 | 20 |
| Acasi 245 | $H_2O$ + 75 wt% Andalusite + 25 wt% haplogranite glass | 12.30 | 750 | 2184 | 1.166 (0.034) | 1.85 | 0.0707 | n.d. | 6.83 | 20 |
| Acasi 66 | $H_2O$ + 75 wt% Andalusite + 25 wt% haplogranite glass | 3.42 | 800 | 480 | 1.090 (0.019) | 1.13 | 0.0742 | n.d. | 2.94 | 15 |
| Acasi 119 | $H_2O$ + 75 wt% Andalusite + 25 wt% haplogranite glass | 3.19 | 800 | 960 | 1.115 (0.030) | 1.30 | 0.0732 | n.d. | 3.23 | 10 |
| Acasi 197 | $H_2O$ + 75 wt% Andalusite + 25 wt% haplogranite glass | 2.84 | 800 | 1100 | 1.125 (0.030) | 1.40 | 0.0748 | n.d. | 3.15 | 20 |
| Acasi 25 | $H_2O$ + 75 wt% Andalusite + 25 wt% haplogranite glass | 44.63 | 800 | 240 | 1.235 (0.039) | 2.68 | 0.0725 | n.d. | 7.11 | 28 |
| Acasi 42 | $H_2O$ + 75 wt% Andalusite + 25 wt% haplogranite glass | 46.06 | 800 | 480 | 1.205 (0.020) | 2.40 | 0.0703 | n.d. | 8.37 | 15 |
| Acasi 75 | $H_2O$ + 75 wt% Andalusite + 25 wt% haplogranite glass | 29.32 | 800 | 480 | 1.207 (0.034) | 2.34 | 0.0742 | n.d. | 6.19 | 10 |
| Acasi 82 | $H_2O$ + 75 wt% Andalusite + 25 wt% haplogranite glass | 19.91 | 800 | 960 | 1.203 (0.024) | 2.30 | 0.0729 | n.d. | 6.39 | 10 |
| Acasi 114 | $H_2O$ + 75 wt% Sillimanite + 25 wt% haplogranite glass | 17.34 | 700 | 4320 | 1.223 (0.034) | 2.32 | 0.0674 | n.d. | 7.86 | 15 |
| Acasi 241 | $H_2O$ + 75 wt% Sillimanite + 25 wt% haplogranite glass | 35.05 | 750 | 2184 | 1.208 (0.030) | 2.31 | 0.0721 | n.d. | 7.37 | 9 |
| Acasi 103 | $H_2O$ + 75 wt% Sillimanite + 25 wt% haplogranite glass | 3.17 | 800 | 960 | 1.188 (0.022) | 2.19 | 0.0798 | n.d. | 3.98 | 10 |
| Acasi 191 | $H_2O$ + 75 wt% Sillimanite + 25 wt% haplogranite glass | 2.99 | 800 | 1100 | 1.146 (0.028) | 1.63 | 0.0747 | n.d. | 3.62 | 20 |
| Acasi 136 | $H_2O$ + 75 wt% Sillimanite + 25 wt% haplogranite glass | 3.49 | 800 | 480 | 1.206 (0.066) | 2.33 | 0.0731 | n.d. | 6.84 | 12 |
| Acasi 137 | $H_2O$ + 75 wt% Sillimanite + 25 wt% haplogranite glass | 12.62 | 800 | 480 | 1.243 (0.025) | 2.63 | 0.0711 | n.d. | 7.65 | 12 |

**Table 2** (Contd.)

| Run no. | Starting materials | $H_2O$[a] (wt%) | Temperature (°C) | Duration (h) | Melt ASI (SD) | Normative corundum | Mole fraction of $Al_2O_3$ | $B_2O_3$ wt% (SD) | $H_2O$[b] (wt%) | No. analyses |
|---|---|---|---|---|---|---|---|---|---|---|
| Acasi 102 | $H_2O$ + 75 wt% Sillimanite + 25 wt% haplogranite glass | 22.07 | 800 | 960 | 1.292 (0.028) | 3.04 | 0.0732 | n.d. | 6.45 | 10 |
| Acasi 190 | $H_2O$ + 75 wt% Sillimanite + 25 wt% haplogranite glass | 13.67 | 800 | 1100 | 1.268 (0.032) | 2.85 | 0.0718 | n.d. | 7.62 | 20 |
| Acasi 40 | $H_2O$ + 75 wt% Kyanite + 25 wt% haplogranite glass | 39.72 | 700 | 480 | 1.177 (0.028) | 1.98 | 0.0667 | n.d. | 8.39 | 15 |
| Acasi 32 | $H_2O$ + 75 wt% Kyanite + 25 wt% haplogranite glass | 28.00 | 700 | 2160 | 1.201 (0.026) | 2.31 | 0.0710 | n.d. | 7.55 | 10 |
| Acasi 160 | $H_2O$ + 75 wt% Kyanite + 25 wt% haplogranite glass | 16.51 | 700 | 4320 | 1.239 (0.039) | 2.52 | 0.0700 | n.d. | 7.79 | 20 |
| Acasi 242 | $H_2O$ + 75 wt% Kyanite + 25 wt% haplogranite glass | 13.89 | 750 | 480 | 1.205 (0.033) | 2.22 | 0.0700 | n.d. | 7.84 | 30 |
| Acasi 256 | $H_2O$ + 75 wt% Kyanite + 25 wt% haplogranite glass | 13.96 | 750 | 1392 | 1.219 (0.031) | 2.02 | 0.0611 | n.d. | 6.12 | 20 |
| Acasi 243 | $H_2O$ + 75 wt% Kyanite + 25 wt% haplogranite glass | 12.34 | 750 | 2184 | 1.212 (0.025) | 2.08 | 0.0650 | n.d. | 6.12 | 20 |
| Acasi 47 | $H_2O$ + 75 wt% Kyanite + 25 wt% haplogranite glass | 3.46 | 800 | 480 | 1.188 (0.025) | 2.17 | 0.0756 | n.d. | 4.76 | 10 |
| Acasi 120 | $H_2O$ + 75 wt% Kyanite + 25 wt% haplogranite glass | 3.18 | 800 | 480 | 1.140 (0.023) | 1.53 | 0.0738 | n.d. | 2.95 | 10 |
| Acasi 141 | $H_2O$ + 75 wt% Kyanite + 25 wt% haplogranite glass | 3.65 | 800 | 960 | 1.141 (0.026) | 1.57 | 0.0727 | n.d. | 4.10 | 10 |
| Acasi 195 | $H_2O$ + 75 wt% Kyanite + 25 wt% haplogranite glass | 3.04 | 800 | 1100 | 1.161 (0.031) | 1.82 | 0.0770 | n.d. | 3.83 | 20 |
| Acasi 23 | $H_2O$ + 75 wt% Kyanite + 25 wt% haplogranite glass | 33.33 | 800 | 240 | 1.292 (0.035) | 3.00 | 0.0699 | n.d. | 6.56 | 31 |
| Acasi 39 | $H_2O$ + 75 wt% Kyanite + 25 wt% haplogranite glass | 31.49 | 800 | 480 | 1.211 (0.026) | 2.50 | 0.0722 | n.d. | 8.92 | 15 |
| Acasi 72 | $H_2O$ + 75 wt% Kyanite + 25 wt% haplogranite glass | 39.96 | 800 | 480 | 1.300 (0.039) | 2.78 | 0.0651 | n.d. | 6.21 | 10 |
| Acasi 83 | $H_2O$ + 75 wt% Kyanite + 25 wt% haplogranite glass | 17.71 | 800 | 960 | 1.266 (0.037) | 2.35 | 0.0611 | n.d. | 5.68 | 10 |
| Acasi 194 | $H_2O$ + 75 wt% Kyanite + 25 wt% haplogranite glass | 10.42 | 800 | 1100 | 1.274 (0.033) | 2.40 | 0.0610 | n.d. | 6.03 | 20 |
| Acasi 46 | $H_2O$ + 50 wt% Muscovite + 50 wt% haplogranite glass | 18.58 | 700 | 480 | 1.271 (0.109) | 2.60 | 0.0625 | n.d. | 8.57 | 7 |
| Acasi 36 | $H_2O$ + 50 wt% Muscovite + 50 wt% haplogranite glass | 28.66 | 700 | 2160 | 1.269 (0.025) | 3.03 | 0.0739 | n.d. | 8.20 | 17 |
| Acasi 117 | $H_2O$ + 50 wt% Muscovite + 50 wt% haplogranite glass | 16.53 | 700 | 4320 | 1.257 (0.032) | 2.69 | 0.0712 | n.d. | 7.77 | 12 |
| Acasi 159 | $H_2O$ + 50 wt% Muscovite + 50 wt% haplogranite glass | 9.23 | 700 | 4320 | 1.107 (0.027) | 1.14 | 0.0638 | n.d. | 6.98 | 20 |
| Acasi 41 | $H_2O$ + 75 wt% Cordierite + 25 wt% haplogranite glass | 32.92 | 700 | 2160 | 1.207 (0.034) | 2.20 | 0.0679 | n.d. | 7.73 | 10 |
| Acasi 131 | $H_2O$ + 75 wt% Cordierite + 25 wt% haplogranite glass | 16.07 | 700 | 4320 | 1.203 (0.024) | 2.19 | 0.0699 | n.d. | 6.98 | 12 |
| Acasi 161 | $H_2O$ + 75 wt% Cordierite + 25 wt% haplogranite glass | 18.57 | 700 | 4320 | 1.209 (0.026) | 2.25 | 0.0696 | n.d. | 7.57 | 20 |
| Acasi 246 | $H_2O$ + 75 wt% Cordierite + 25 wt% haplogranite glass | 15.60 | 750 | 480 | 1.173 (0.066) | 2.01 | 0.0743 | n.d. | 8.22 | 30 |
| Acasi 255 | $H_2O$ + 75 wt% Cordierite + 25 wt% haplogranite glass | 21.34 | 750 | 1392 | 1.195 (0.050) | 2.17 | 0.0717 | n.d. | 6.86 | 20 |
| Acasi 247 | $H_2O$ + 75 wt% Cordierite + 25 wt% haplogranite glass | 13.32 | 750 | 2184 | 1.180 (0.031) | 2.03 | 0.0733 | n.d. | 6.06 | 20 |
| Acasi 67 | $H_2O$ + 75 wt% Cordierite + 25 wt% haplogranite glass | 3.33 | 800 | 480 | 1.111 (0.023) | 1.44 | 0.0776 | n.d. | 4.19 | 10 |
| Acasi 101 | $H_2O$ + 75 wt% Cordierite + 25 wt% haplogranite glass | 3.30 | 800 | 960 | 1.175 (0.022) | 2.06 | 0.0789 | n.d. | 4.21 | 10 |
| Acasi 192 | $H_2O$ + 75 wt% Cordierite + 25 wt% haplogranite glass | 3.03 | 800 | 1100 | 1.132 (0.020) | 1.51 | 0.0751 | n.d. | 3.75 | 20 |
| Acasi 53 | $H_2O$ + 75 wt% Cordierite + 25 wt% haplogranite glass | 32.78 | 800 | 240 | 1.208 (0.037) | 2.40 | 0.0713 | n.d. | 7.64 | 11 |
| Acasi 30 | $H_2O$ + 75 wt% Cordierite + 25 wt% haplogranite glass | 37.41 | 800 | 480 | 1.272 (0.045) | 2.89 | 0.0700 | n.d. | 8.83 | 15 |
| Acasi 73 | $H_2O$ + 75 wt% Cordierite + 25 wt% haplogranite glass | 34.93 | 800 | 480 | 1.305 (0.024) | 3.38 | 0.0795 | n.d. | 5.85 | 10 |
| Acasi 81 | $H_2O$ + 75 wt% Cordierite + 25 wt% haplogranite glass | 23.22 | 800 | 960 | 1.286 (0.026) | 3.17 | 0.0752 | n.d. | 6.92 | 10 |
| Acasi 193 | $H_2O$ + 75 wt% Cordierite + 25 wt% haplogranite glass | 10.40 | 800 | 1100 | 1.198 (0.033) | 2.22 | 0.0746 | n.d. | 5.72 | 20 |
| Acasi 126 | $H_2O$ + 75 wt% Tourmaline + 25 wt% haplogranite glass | 10.84 | 700 | 4320 | 1.262 (0.027) | 2.80 | 0.0752 | 0.67 (0.21) | 7.07 | 20 |
| Acasi 147–2 | $H_2O$ + 75 wt% Tourmaline + 25 wt% haplogranite glass | 14.72 | 700 | 4320 | 1.298 (0.025) | 3.13 | 0.0754 | 1.66 (0.25) | 6.18 | 20 |
| Acasi 249 | $H_2O$ + 75 wt% Tourmaline + 25 wt% haplogranite glass | 13.61 | 750 | 480 | 1.291 (0.040) | 3.07 | | n.d. | | 30 |
| Acasi 254 | $H_2O$ + 75 wt% Tourmaline + 25 wt% haplogranite glass | 18.20 | 750 | 1392 | 1.273 (0.030) | 2.89 | | n.d. | | 20 |
| Acasi 248 | $H_2O$ + 75 wt% Tourmaline + 25 wt% haplogranite glass | 12.60 | 750 | 2184 | 1.298 (0.051) | 3.05 | | n.d. | | 20 |
| Acasi 138 | $H_2O$ + 75 wt% Tourmaline + 25 wt% haplogranite glass | 3.58 | 800 | 960 | 1.167 (0.016) | 2.39 | 0.0753 | 1.03 (0.29) | 3.06 | 10 |
| Acasi 139 | $H_2O$ + 75 wt% Tourmaline + 25 wt% haplogranite glass | 3.14 | 800 | 1100 | 1.264 (0.036) | 2.94 | 0.0841 | 2.51 (1.13) | 2.92 | 20 |
| Acasi 140 | $H_2O$ + 75 wt% Tourmaline + 25 wt% haplogranite glass | 11.89 | 800 | 480 | 1.435 (0.027) | 4.40 | 0.0773 | 4.23 (0.39) | 6.09 | 12 |
| Acasi 104 | $H_2O$ + 75 wt% Tourmaline + 25 wt% haplogranite glass | 17.83 | 800 | 960 | 1.422 (0.037) | 4.09 | 0.0742 | 3.11 (0.26) | 7.11 | 10 |
| Acasi 127 | $H_2O$ + 75 wt% Tourmaline + 25 wt% haplogranite glass | 15.99 | 800 | 960 | 1.442 (0.025) | 4.43 | 0.0728 | 4.08 (0.25) | 7.38 | 10 |
| Acasi 187 | $H_2O$ + 75 wt% Tourmaline + 25 wt% haplogranite glass | 13.60 | 800 | 1100 | 1.426 (0.029) | 4.13 | 0.0763 | 4.34 (0.49) | 6.05 | 20 |

[a]Proportion of water sealed inside the capsule with respect to the haplogranite glass
[b]$H_2O$ calculated by the EMPA difference method

**Table 3** Electron microprobe analyses (wt%) of a high-silica topaz rhyolitic glass at different analytical conditions. All elements were analyzed for 30 s on peak using 20 kV acceleration. Sodium and aluminum were always analyzed first and concurrently

| Beam conditions<br>No. analyses | 2 nA, 20 μm<br>8 | 2 nA, 5 μm<br>8 | 20 nA, 5 μm<br>8 |
|---|---|---|---|
| $SiO_2$ | 70.54 (0.26) | 71.30 (0.68) | 71.41 (0.56) |
| $Al_2O_3$ | 12.30 (0.14) | 12.29 (0.22) | 12.29 (0.14) |
| CaO | 1.16 (0.06) | 1.17 (0.06) | 1.17 (0.05) |
| $Na_2O$ | 4.10 (0.15) | 3.71 (0.41) | 2.07 (0.12) |
| $K_2O$ | 3.50 (0.08) | 3.48 (0.08) | 3.41 (0.06) |
| Total | 91.60 (0.21) | 91.95 (0.78) | 90.35 (0.61) |
| ASI | 0.974 (0.027) | 1.027 (0.051) | 1.334 (0.032) |

of corundum fibers/plates in the melt close to mineral grain boundaries (Fig. 1h, i), but this was not observed in andalusite or sillimanite dissolution runs. Sillimanite dissolution runs produced euhedral cordierite and ilmenite at mineral boundaries (Fig. 1j), with FeO, MgO and $TiO_2$ apparently supplied by inclusions of biotite and ilmenite in the sillimanite. Upon dissolution of tourmaline, euhedral corundum, aluminosilicate, cordierite and hercynite crystallized, accompanied by sporadic euhedral overgrowths of new tourmaline on relict grains (Fig. 1k, l).

## Chemical composition of glasses

ASI values, normative corundum, mole fractions of $Al_2O_3$, as well as $B_2O_3$ and $H_2O$ concentrations for all experimental glasses are listed in Table 2. Representative complete chemical analyses of experimental glasses are presented in Tables 5, 6, 7. Plots of ASI versus $H_2O$ concentration of glass for all run products at 800 °C, and ASI versus temperature for $H_2O$-saturated experiments are shown in Figs. 2 and 3, respectively. Temperature and especially $H_2O$ have a notable influence on the ASI of the melt. ASI increases by 0.10 to 0.20 units as the concentration of $H_2O$ in melt increases from ≈3 to 7 wt%. Although not quantified, a positive correlation between ASI and $H_2O$ concentration of granitic melts was reported by Clemens and Wall (1981) and Dingwell et al. (1997), and also was suggested by Patiño Douce (1992) on the basis of previously published experimental data. Based on the data for corundum, kyanite, and cordierite, the relationship between these two variables is described with the equation of a straight line. Linear regression of the current data using ASI as the dependent variable (Fig. 2) yields a range of increase in ASI of 0.025 to 0.050 units per 1 wt% $H_2O$, corresponding to a ratio of 0.04–0.10 moles of excess $Al_2O_3$ per mole of $H_2O$. This regression also yields an ASI value of ≈1.00–1.10 for anhydrous liquids, which is consistent with previous experimental studies by Schairer and Bowen (1955, 1956). On the other hand, regression of the data from $H_2O$-saturated 800 °C experiments treating $H_2O$ as the dependent variable yields increases in $H_2O$ in liquid of ≈2 moles per mole of excess $Al_2O_3$, and $H_2O$ concentrations of ≈6.3 wt% for melts with an ASI = 1.00; both of these observations also are consistent with previous investigations of $H_2O$ saturation in granitic melts (Dingwell et al. 1984, 1997; Holtz et al. 1992a, 1992b, 1992c, 1995; Linnen et al. 1996; Behrens and Jantos 2001).

ASI does not vary perceptibly between 700 and 750 °C at $H_2O$-saturated conditions, but increases from 750 to 800 °C in liquids coexisting with andalusite, sillimanite, kyanite, cordierite and tourmaline (Fig. 3). ASI of melts coexisting with corundum, however, show nominally no dependence on temperature. Exponential functions have been used to model the relationship between ASI and temperature (Fig. 3). The curvatures in these ASI-$T$ plots reflect the curvatures in the liquidus surfaces of the peraluminous phases: the slope of the liquidus surface in $X$-$T$ space is the inverse of the $T$-$X$ section most familiar to petrologists.

Figures 2 and 3 also illustrate that ASI increases with the chemical complexity of the dissolving peraluminous phase, i.e. with addition of FeO, MgO and $B_2O_3$ to the system. For example, at 6.5 wt% $H_2O$ and 800 °C, melt ASI is ≈1.19 for experiments containing only added

**Table 4** $H_2O$ concentrations (wt%) by EMPA-difference versus other methods

| Method<br>Sample/reference | $H_2O$ EMPA-diff<br>This work | $H_2O$ EMPA-diff<br>Morgan and London (1996) | $H_2O$ by FTIR<br>Silver and Stolper (1989) | H2O by SIMS<br>This work | $H_2O$ by KFT<br>Holtz et al. (1992) | $H_2O$ by KFT<br>Behrens and Jantos (2001) |
|---|---|---|---|---|---|---|
| A1009 | 2.39 | 2.46 | 2.22 | | | |
| ABC-11 | 5.63 | 5.48 | 4.94 | | | |
| LAS-21 | 10.30 | 9.80 | 9.65 | | | |
| Acasi 91 | 7.21 | | | 5.42 | | |
| Acasi 135 | 3.54 | | | 3.47 | | |
| Acasi 101 | 4.21 | | | 4.21 | | |
| Acasi 81 | 6.92 | | | 5.52 | | |
| Acasi 104 | 7.11 | | | 6.50 | | |
| Acasi 138 | 3.06 | | | 3.73 | | |
| CG-1 ($Ab_{38}Or_{29}Qtz_{34}$) | 6.51 | | | | | |
| HPG 8 ($Ab_{39}Or_{25}Qtz_{36}$) | | | | | 5.94 | |
| Schott R ($Ab_{38}Or_{34}Qtz_{28}$) | | | | | 5.83 | |
| EDF ($Ab_{36}Or_{29}Qtz_{35}$) | | | | | | 6.26 |
| LGB ($Ab_{35}Or_{28}Qtz_{37}$) | | | | | | 6.21 |
| BL ($Ab_{35}Or_{23}Qtz_{42}$) | | | | | | 6.21 |

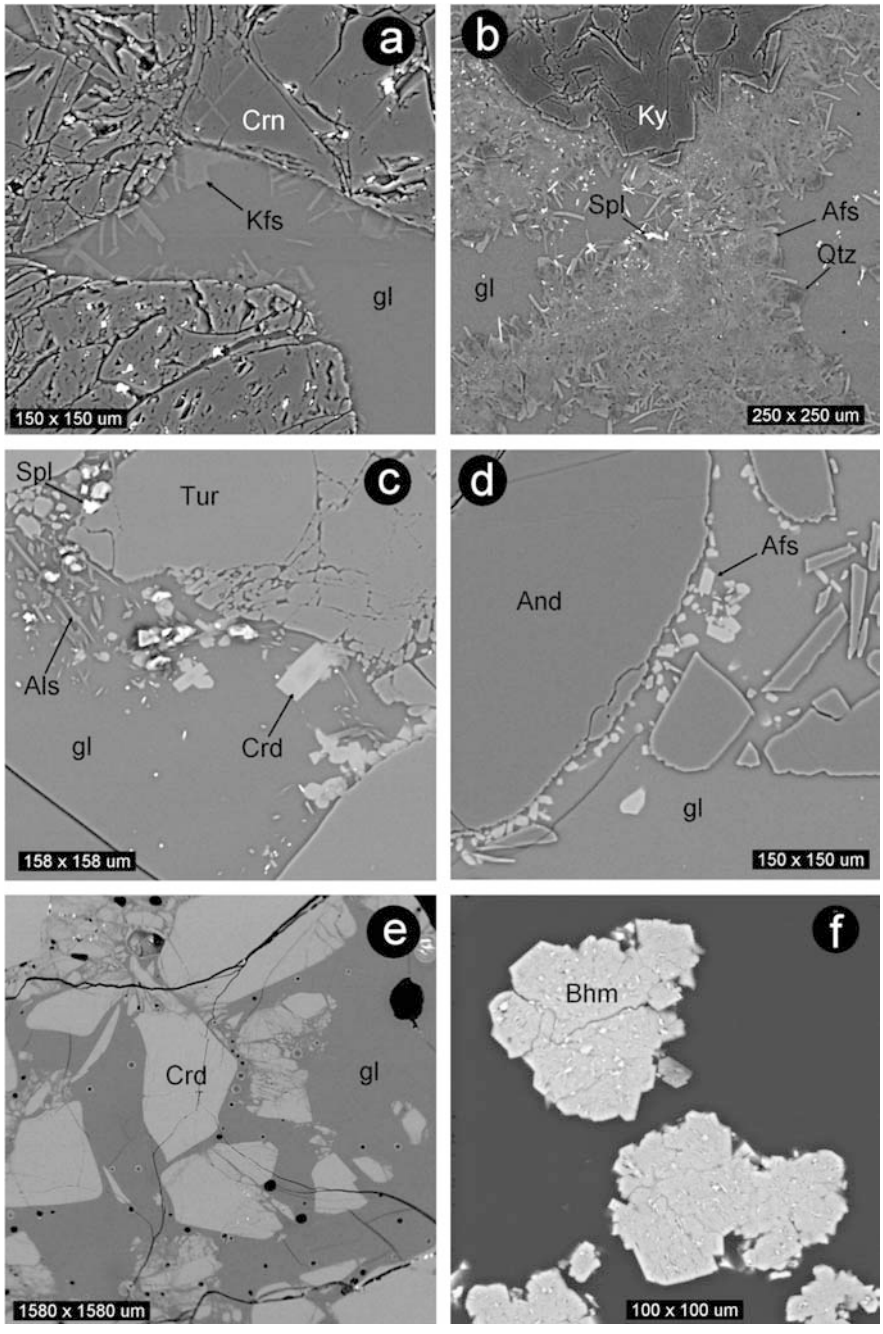


**Fig. 1** Backscattered electron images of selected experimental run products. Abbreviations for minerals after Kretz (1983). *Afs* Alkali feldspar, *gl* glass. **a** Acasi 121. **b** Acasi 141. **c** Acasi 139. **d** Acasi 112. **e** Acasi 193. **g** Acasi 134. **h, i** Acasi 194. **j** Acasi 102. **k**, **l** Acasi 187. See text for explanation

corundum, ≈1.25 for experiments with added cordierite, and ≈1.44 for experiments with added tourmaline.

The same tendencies described above are observed when, instead of ASI, concentration of normative corundum is used as measure of the peraluminous character of the melt (Figs. 4, 5). The mole fraction of $Al_2O_3$, on the other hand, tends to remain constant or decrease with increasing $H_2O$ concentration, but to increase with increasing temperature.

## Approach to equilibrium

It is essential to assess if equilibrium was achieved in the experiments, in order to apply these data meaningfully to natural systems. Several observations are consistent with a close approach to equilibrium between minerals and melt:

1. The composition of experimental glasses is homogeneous within analytical errors (see standard deviations in Tables 5, 6, 7, Fig. 6). This observation indicates that diffusion has erased any initial compositional gradients and, possibly, that equilibrium has been achieved.
2. Glasses from experiments of increasing duration (480 to 2,160 to 4,320 h at 700 °C, and 240 to 480 to 960 h at 800 °C) run under the same conditions of temperature, pressure and melt $H_2O$ content, show comparable ASI values and compositions. Sillimanite

**Fig. 1** (Contd.)

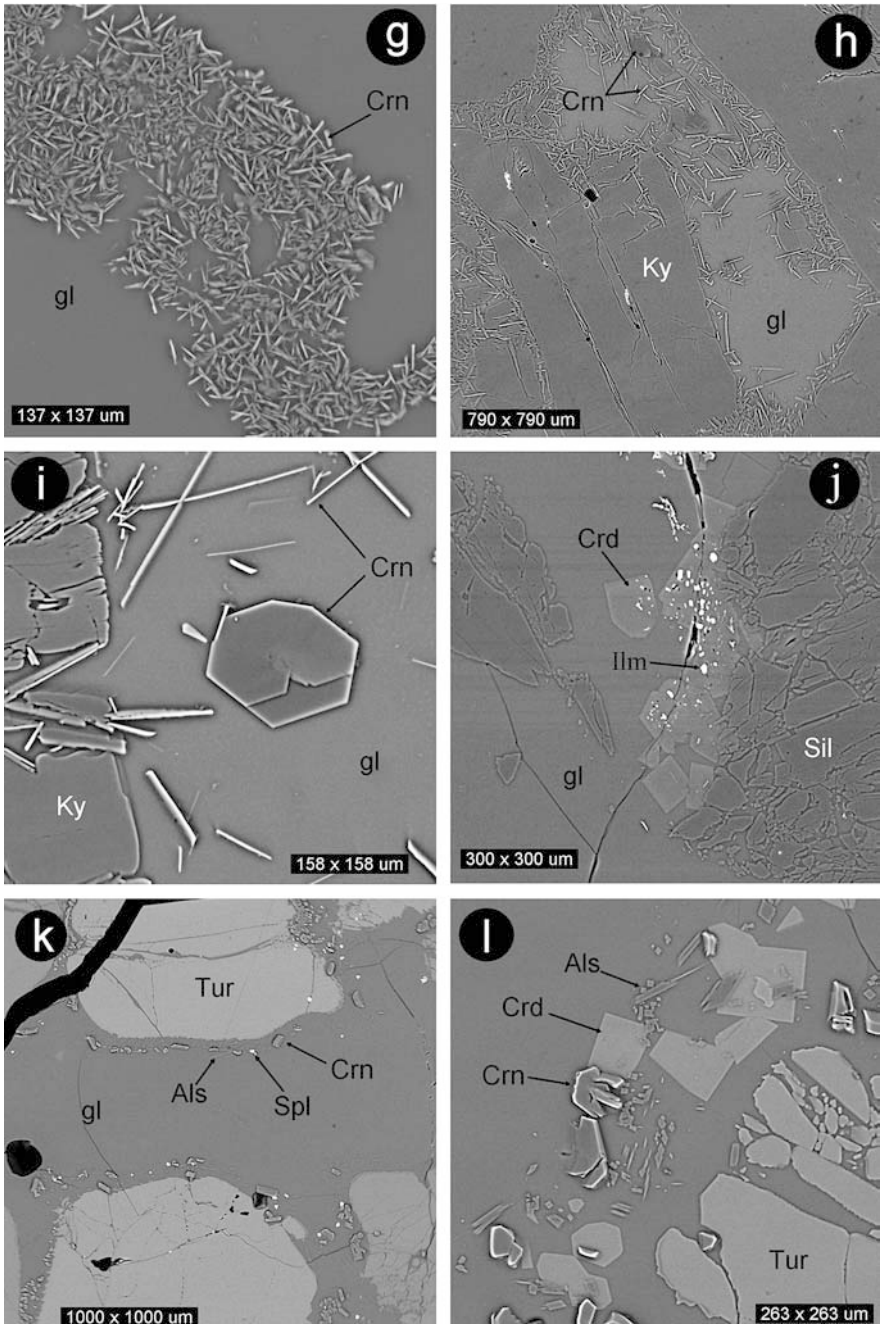


and cordierite dissolution experiments at 800 °C are exceptions, suggesting slightly slower dissolution kinetics with respect to corundum, andalusite, kyanite or tourmaline.

3. In runs with boehmite powder as the source of excess aluminum, boehmite was transformed into fibrous to platy corundum 2 to 10 μm in grain size, as confirmed by X-ray diffraction and BSE imaging (Fig. 1f, g). The initial intent of these experiments was to reverse the corundum dissolution runs via the dissolution of boehmite into the melt and re-precipitation as corundum. The ASI values of these experimental glasses are comparable to those obtained in corundum dissolution runs (Table 2, Figs. 2 and 3), even though the reactive surface of boehmite was orders of magnitude greater.
4. Upon dissolution of the starting peraluminous minerals, some experiments show growth of new, euhedral peraluminous phases in melt close to, or on, relict aluminous minerals, as described above. This indicates saturation of the melt in these new minerals, both in terms of direct precipitation from the melt and as the result of peritectic reactions.
5. At the current experimental conditions, sillimanite is the stable aluminosilicate in equilibrium with (quartz-saturated) liquid, but was not produced by dissolution of andalusite or kyanite. Lack of sillimanite production accompanying andalusite dissolution could be

**Table 5** Representative compositions (wt%) of glasses in $H_2O$-saturated experiments conducted at 800 °C and 200 MPa

| Starting peraluminous mineral<br>Run no. | Corundum<br>Acasi 188 | Boehmite<br>Acasi 167 | Andalusite<br>Acasi 82 | Sillimanite<br>Acasi 102 | Kyanite<br>Acasi 194 | Cordierite<br>Acasi 81 | Tourmaline<br>Acasi 104 |
|---|---|---|---|---|---|---|---|
| $SiO_2$ | 71.42 (0.69) | 71.22 (0.27) | 71.79 (0.60) | 71.71 (0.67) | 76.19 (0.73) | 70.36 (0.61) | 67.39 (0.39) |
| $TiO_2$ | n.d. | n.d. | 0.01 (0.01) | 0.11 (0.02) | n.d. | 0.01 (0.01) | 0.02 (0.02) |
| $Al_2O_3$ | 13.38 (0.26) | 13.71 (0.21) | 13.13 (0.13) | 13.38 (0.21) | 11.19 (0.21) | 13.89 (0.11) | 13.73 (0.22) |
| FeO[a] | 0.02 (0.01) | n.d. | 0.09 (0.02) | 0.12 (0.03) | 0.03 (0.01) | 0.55 (0.07) | 0.62 (0.06) |
| MnO | 0.00 (0.00) | n.d. | 0.01 (0.01) | 0.02 (0.01) | 0.00 (0.00) | 0.03 (0.01) | 0.53 (0.02) |
| MgO | 0.02 (0.01) | n.d. | 0.07 (0.02) | 0.22 (0.01) | 0.02 (0.01) | 0.20 (0.01) | 0.30 (0.01) |
| CaO | 0.02 (0.01) | 0.03 (0.02) | 0.03 (0.05) | 0.04 (0.02) | 0.02 (0.02) | 0.04 (0.04) | 0.06 (0.02) |
| BaO | 0.01 (0.01) | n.d. | 0.02 (0.02) | 0.02 (0.01) | 0.01 (0.01) | 0.01 (0.01) | 0.01 (0.01) |
| $Na_2O$ | 4.01 (0.12) | 4.12 (0.10) | 3.89 (0.09) | 3.09 (0.12) | 3.10 (0.10) | 3.87 (0.08) | 3.45 (0.08) |
| $K_2O$ | 4.39 (0.11) | 4.41 (0.11) | 4.28 (0.12) | 4.81 (0.06) | 3.38 (0.10) | 4.02 (0.11) | 3.58 (0.10) |
| $P_2O_5$ | n.d. | n.d. | 0.07 (0.04) | 0.01 (0.01) | n.d. | 0.07 (0.02) | 0.01 (0.01) |
| $B_2O_3$ | n.d. | n.d. | n.d. | n.d. | n.d. | n.d. | 3.11 (0.26) |
| F | 0.02 (0.03) | n.d. | 0.02 (0.03) | 0.04 (0.03) | 0.04 (0.04) | 0.03 (0.02) | 0.13 (0.05) |
| Cl | n.d. | n.d. | 0.01 (0.01) | 0.01 (0.01) | n.d. | 0.01 (0.00) | 0.01 (0.00) |
| F = O | −0.01 | | −0.01 | −0.02 | −0.02 | −0.01 | −0.06 |
| Cl = O | | | 0.00 | 0.00 | | 0.00 | 0.00 |
| $H_2O$ by diff. | 6.70 | 6.52 | 6.39 | 6.45 | 6.03 | 6.92 | 7.11 |
| ASI | 1.175 | 1.181 | 1.203 | 1.292 | 1.274 | 1.286 | 1.422 |
| X $Al_2O_3$(hyd)[b] | 0.0727 | 0.0749 | 0.0729 | 0.0732 | 0.0610 | 0.0752 | 0.0742 |
| Normative corundum | 1.99 | 2.10 | 2.30 | 3.04 | 2.40 | 3.17 | 4.09 |

[a]Total Fe as FeO
[b]Molar fraction of $Al_2O_3$ considering $H_2O$

**Table 6** Representative compositions (wt%) of glasses in $H_2O$-undersaturated experiments conducted at 800 °C and 200 MPa

| Starting peraluminous mineral<br>Run no. | Corundum<br>Acasi 189 | Boehmite<br>Acasi 94 | Andalusite<br>Acasi 119 | Sillimanite<br>Acasi 103 | Kyanite<br>Acasi 195 | Cordierite<br>Acasi 101 | Tourmaline<br>Acasi 139 |
|---|---|---|---|---|---|---|---|
| $SiO_2$ | 75.66 (0.48) | 75.77 (0.41) | 75.83 (0.50) | 72.54 (0.28) | 74.31 (0.36) | 72.82 (0.47) | 71.03 (1.98) |
| $TiO_2$ | n.d. | n.d. | 0.01 (0.01) | 0.11 (0.05) | n.d. | 0.02 (0.01) | 0.02 (0.02) |
| $Al_2O_3$ | 12.60 (0.23) | 12.56 (0.18) | 12.50 (0.10) | 13.74 (0.19) | 13.29 (0.21) | 13.72 (0.27) | 14.11 (0.74) |
| FeO[a] | 0.03 (0.01) | n.d. | 0.02 (0.01) | 0.57 (0.12) | 0.02 (0.01) | 0.53 (0.06) | 0.49 (0.13) |
| MnO | 0.00 (0.00) | n.d. | 0.00 (0.00) | 0.02 (0.01) | 0.00 (0.00) | 0.02 (0.01) | 0.56 (0.14) |
| MgO | 0.01 (0.01) | n.d. | 0.01 (0.00) | 0.13 (0.01) | 0.01 (0.01) | 0.12 (0.01) | 0.07 (0.02) |
| CaO | 0.01 (0.01) | 0.00 (0.01) | 0.01 (0.02) | 0.05 (0.03) | 0.02 (0.02) | 0.02 (0.01) | 0.03 (0.01) |
| BaO | 0.01 (0.01) | n.d. | 0.00 (0.01) | 0.01 (0.01) | 0.01 (0.01) | 0.01 (0.01) | n.d. |
| $Na_2O$ | 3.94 (0.15) | 4.05 (0.10) | 3.86 (0.16) | 3.46 (0.09) | 3.99 (0.14) | 4.34 (0.16) | 4.00 (0.25) |
| $K_2O$ | 4.44 (0.10) | 4.42 (0.10) | 4.48 (0.09) | 5.35 (0.12) | 4.50 (0.09) | 4.16 (0.08) | 4.19 (0.19) |
| $P_2O_5$ | n.d. | n.d. | 0.01 (0.01) | 0.01 (0.01) | n.d. | n.d. | 0.01 (0.01) |
| $B_2O_3$ | n.d. | n.d. | n.d. | n.d. | n.d. | n.d. | 2.51 (1.13) |
| F | 0.02 (0.03) | n.d. | 0.03 (0.03) | 0.07 (0.05) | 0.04 (0.04) | 0.02 (0.02) | 0.11 (0.03) |
| Cl | n.d. | n.d. | 0.02 (0.01) | 0.02 (0.01) | n.d. | 0.01 (0.01) | n.d. |
| F = O | −0.01 | | −0.01 | −0.03 | −0.02 | −0.01 | −0.05 |
| Cl = O | | | 0.00 | 0.00 | | 0.00 | |
| $H_2O$ by diff. | 3.29 | 3.19 | 3.23 | 3.98 | 3.83 | 4.21 | 2.92 |
| ASI | 1.115 | 1.096 | 1.115 | 1.188 | 1.161 | 1.175 | 1.264 |
| $XAl_2O_3$ (hyd)[b] | 0.0737 | 0.0734 | 0.0732 | 0.0798 | 0.0770 | 0.0789 | 0.0841 |
| Normative corundum | 1.29 | 1.15 | 1.30 | 2.19 | 1.82 | 2.06 | 2.94 |

[a]Total Fe as FeO
[b]Molar fraction of $Al_2O_3$ considering $H_2O$

explained by the observation that the Gibbs free energy change for the reaction andalusite = sillimanite is negligible at these temperature-pressure conditions (and also is approximately equivalent to the errors associated with measurement of the thermodynamic quantities: Acosta-Vigil et al. 2002). The dissolution of kyanite (but not andalusite or sillimanite) resulted in the precipitation of corundum. More rapid reaction of kyanite could be due to the fact that it is farther from its stability field than are andalusite or sillimanite, and production of corundum likely results from reaction along the metastable extension of the kyanite = corundum + quartz reaction boundary in the sillimanite field (Harlov and Milke 2002).

**Table 7** Representative compositions (wt%) of glasses in $H_2O$-saturated experiments conducted at 700 °C and 200 MPa

| Starting peraluminous mineral<br>Run no. | Corundum<br>Acasi 113 | Boehmite<br>Acasi 116 | Andalusite<br>Acasi 112 | Sillimanite<br>Acasi 114 | Kyanite<br>Acasi 160 | Muscovite<br>Acasi 36 | Cordierite<br>Acasi 131 | Tourmaline<br>Acasi 126 |
|---|---|---|---|---|---|---|---|---|
| $SiO_2$ | 71.68 (0.33) | 71.67 (0.36) | 71.96 (0.51) | 71.33 (0.41) | 71.00 (0.59) | 69.10 (0.48) | 71.70 (0.30) | 70.18 (0.51) |
| $TiO_2$ | n.d. | n.d. | n.d. | n.d | n.d. | 0.03 (0.01) | 0.01 (0.01) | 0.02 (0.02) |
| $Al_2O_3$ | 12.92 (0.21) | 12.98 (0.13) | 12.71 (0.14) | 12.74 (0.20) | 13.20 (0.18) | 13.99 (0.16) | 12.98 (0.18) | 13.50 (0.19) |
| FeO[a] | n.d. | n.d. | n.d. | 0.01 (0.01) | 0.01 (0.01) | 0.22 (0.01) | 0.29 (0.03) | 0.36 (0.04) |
| MnO | n.d. | n.d. | n.d. | 0.01 (0.01) | 0.00 (0.00) | 0.02 (0.01) | 0.01 (0.01) | 0.19 (0.02) |
| MgO | n.d. | n.d. | n.d. | 0.13 (0.01) | 0.02 (0.00) | 0.05 (0.01) | 0.10 (0.01) | 0.06 (0.01) |
| CaO | 0.03 (0.02) | 0.02 (0.01) | 0.02 (0.02) | 0.08 (0.03) | 0.02 (0.02) | 0.09 (0.03) | 0.03 (0.02) | 0.03 (0.02) |
| BaO | n.d. | n.d. | n.d. | 0.01 (0.01) | 0.00 (0.00) | 0.01 (0.02) | n.d. | n.d. |
| $Na_2O$ | 3.87 (0.10) | 3.94 (0.14) | 3.85 (0.13) | 3.21 (0.10) | 3.64 (0.17) | 3.66 (0.08) | 3.90 (0.10) | 3.70 (0.12) |
| $K_2O$ | 4.23 (0.12) | 4.24 (0.10) | 4.26 (0.09) | 4.61 (0.14) | 4.30 (0.10) | 4.48 (0.11) | 3.99 (0.08) | 4.21 (0.09) |
| $P_2O_5$ | n.d. | n.d. | n.d. | n.d | n.d. | 0.03 (0.02) | n.d. | n.d. |
| $B_2O_3$ | n.d. | n.d. | n.d. | n.d. | n.d. | n.d. | n.d. | 0.67 (0.21) |
| F | n.d. | n.d. | n.d. | 0.03 (0.03) | 0.02 (0.03) | 0.20 (0.03) | 0.01 (0.02) | 0.03 (0.04) |
| Cl | n.d. | n.d. | n.d. | n.d. | n.d. | 0.01 (0.01) | n.d. | n.d. |
| F = O | | | | −0.01 | −0.01 | −0.08 | 0.00 | −0.01 |
| Cl = O | | | | | | 0.00 | | |
| $H_2O$ by diff | 7.27 | 7.15 | 7.21 | 7.86 | 7.79 | 8.20 | 6.98 | 7.07 |
| ASI | 1.175 | 1.170 | 1.160 | 1.223 | 1.239 | 1.269 | 1.203 | 1.263 |
| $XAl_2O_3$(hyd)[b] | 0.0692 | 0.0697 | 0.0681 | 0.0674 | 0.0700 | 0.0739 | 0.0699 | 0.0752 |
| Normative corundum | 1.92 | 1.87 | 1.73 | 2.32 | 2.52 | 3.03 | 2.19 | 2.80 |

[a]Total Fe as FeO
[b]Molar fraction of $Al_2O_3$ considering $H_2O$

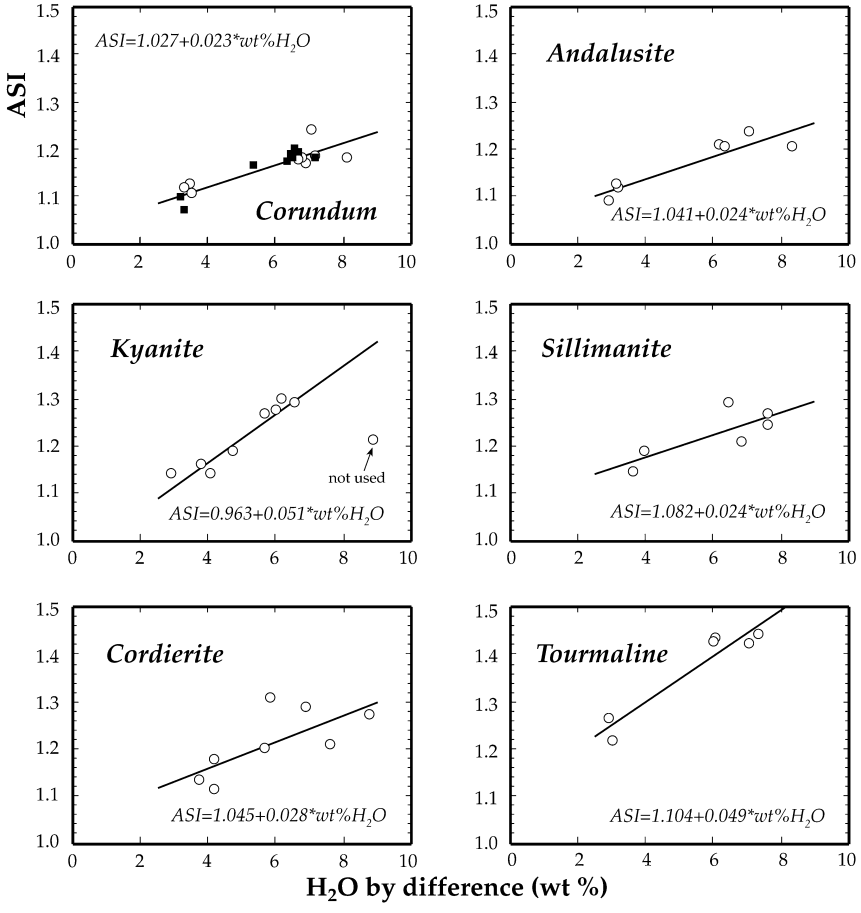


**Fig. 2** ASI values versus $H_2O$ concentration (by EMPA-difference) for resultant experimental glasses coexisting with different peraluminous minerals. Equations for the linear regressions are also shown. Here and thereafter, *squares* and *circles* in the corundum glasses refer to experiments with boehmite and corundum as the starting peraluminous mineral phase, respectively; and *not used* refers to experiments not included in the regressions because their results constitute clear outliers

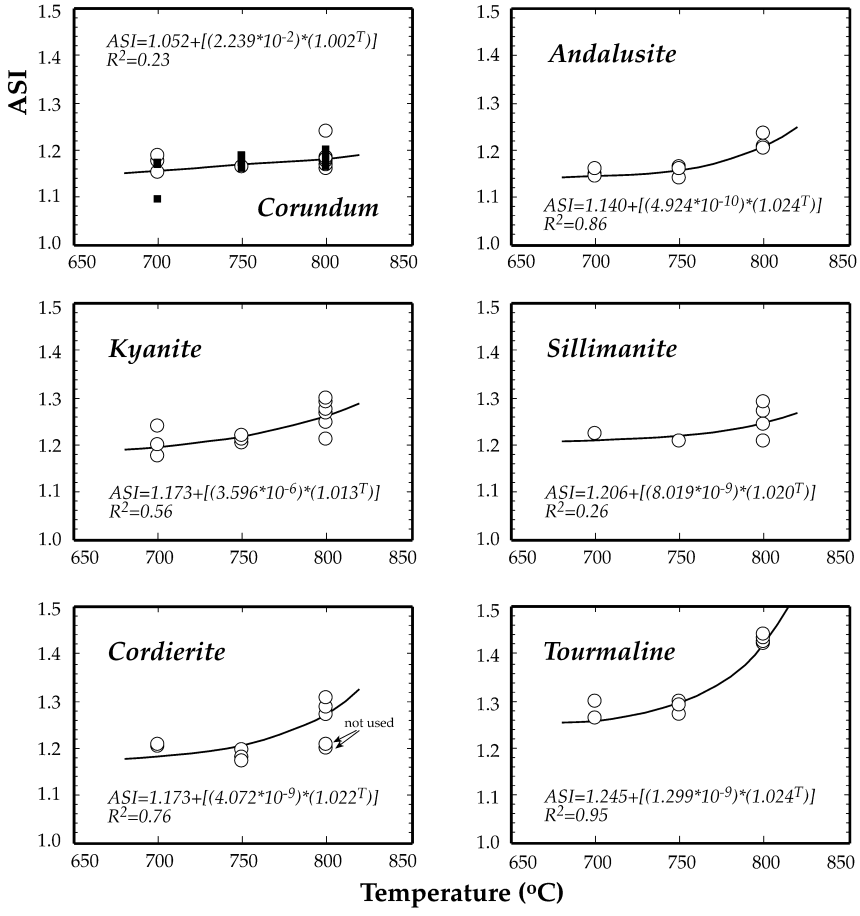


**Fig. 3** ASI values versus temperature for experimental glasses coexisting with different peraluminous minerals. Equations for the exponential fits are also shown

## Discussion

### Utility of the ASI parameter and the concentration of normative corundum

Corundum is the alumina-saturating phase in silicate melts, though the aluminosilicates, rather than corundum, are prevalent in granites because of their quartz-rich compositions (e.g., Weill 1966; Clemens and Wall 1981; Patiño Douce 1992). For the case of corundum, the relevant equilibrium can be written as:

$$a\mathrm{Al_2O_3}\ (\mathrm{Corundum}) = a\mathrm{Al_2O_3}(\mathrm{Melt}) = \gamma\mathrm{Al_2O_3}\ (\mathrm{Melt}) \times X\mathrm{Al_2O_3}\ (\mathrm{Melt}) \quad (1)$$

where $a\mathrm{Al_2O_3}$, $\gamma\mathrm{Al_2O_3}$, and $X\mathrm{Al_2O_3}$ refer to activity, activity coefficient, and molar fraction of $\mathrm{Al_2O_3}$, respectively. Although it would be desirable to know the activity of $\mathrm{Al_2O_3}$ in melt and to correlate it with respect to intensive and extensive thermodynamic variables, $a\mathrm{Al_2O_3}$ (Melt) cannot be calculated directly from chemical analyses of experimental glasses or rocks. If $X\mathrm{Al_2O_3}$ (Melt) is taken as a bulk component of melt, then $\gamma\mathrm{Al_2O_3}$ (Melt) varies with speciation reactions involving Al and other components (as indicated by this current research); therefore, $\gamma\mathrm{Al_2O_3}$ (Melt) cannot be assumed to be near unity and it cannot be readily evaluated. Moreover, the speciation of excess aluminum is still a matter of speculation for anhydrous melts (e.g., Lacy 1963; Mysen et al. 1981; Sato et al. 1991; Poe et al. 1992), and the little that is known about Al speciation in hydrous melts suggests a fundamentally different solution mechanism than for anhydrous melts (e.g., Mungall et al. 1998; Acosta-Vigil et al. 2002). Boron, F, and P exhibit strong interactions with Al (e.g., London et al. 1993, Wolf and London 1997), and these components tend to be important in the peraluminous granites to which these experiments apply. ASI and the concentration of normative corundum, on the other hand, may constitute very useful parameters to extract petrogenetic information of granitic rocks. This is because (1) they can be easily obtained from the chemical analysis of a rock, and (2) our experiments indicate that they vary regularly with temperature and compositional variables.

### Effect of compositional variables on the dissolution of excess alumina in melt

#### *Effects of $H_2O$*

In accordance with the diffusion experiments of Mungall et al. (1998), Acosta-Vigil et al. (2002) obtained tentative

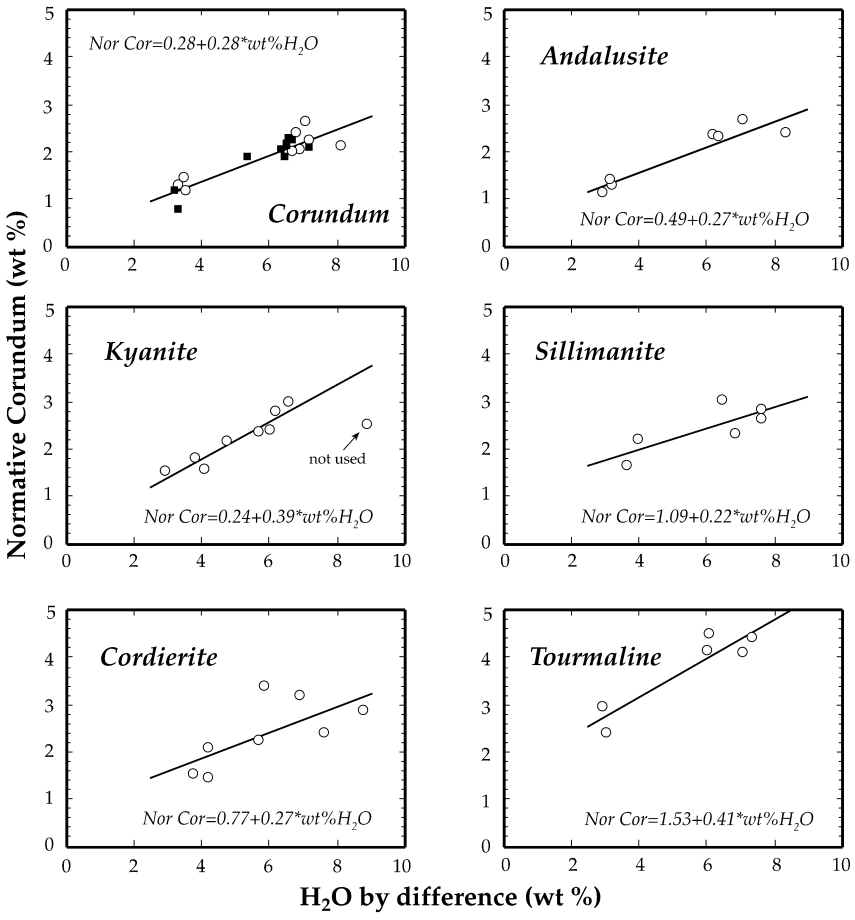


**Fig. 4** Concentrations of normative corundum versus $H_2O$ (measured by EMPA-difference) for resultant experimental glasses coexisting with different peraluminous minerals

evidence that $H_2O$ was a component of a peraluminous species diffusing through melt. This association was suggested by the positive correlation of $H_2O$ with ASI of melt and by similar concentration profiles for $Al_2O_3$ and $H_2O$. With the completion of these new experiments, we can state unequivocally that $H_2O$ is an important variable in promoting the dissolution of excess alumina in melt. Though others have noted an increased solubility of $H_2O$ with excess alumina in $H_2O$-saturated granitic melts (e.g., Dingwell et al. 1984, 1997; Holtz et al. 1992a; Linnen et al. 1996; Behrens and Jantos 2001), we have inverted the relationship to demonstrate the important effect of $XH_2O$ on the solubility of peraluminous phases and the ASI values of melts in equilibrium with them. The effect of $H_2O$ in increasing the peraluminous character of melt, as reflected by the ASI or the concentration of normative corundum, is the single most important observation from this study.

### *Effects of mafic components and boron*

The current data demonstrate a clear trend of increasing solubility of excess alumina with increasing chemical complexity of the melt. This is shown by the higher melt ASI values in cordierite experiments relative to corundum and andalusite experiments, and higher ASI values in tourmaline experiments relative to cordierite experiments at similar $P$–$T$–$XH_2O$ conditions. This indicates that the addition of Fe, Mg, and B facilitates the dissolution of additional excess alumina in melt. Cordierite and tourmaline contribute an Mg* (molar Mg/[Mg + Fe]) of 0.66 and 0.30, respectively, to the melt (Table 1). The increase in ASI with mafic components cannot, therefore, be uniquely ascribed to Mg or Fe in these experiments, and we cannot uniquely separate effects of changing Mg* from the addition of B. Current knowledge about the structural roles of mafic components and B in granitic melts, however, does not provide a clear explanation for the increase in the solubility of alumina with addition of these components (e.g., Dickenson and Hess 1981; Mysen et al. 1985; Virgo and Mysen 1985; Mysen 1987; Gwinn and Hess 1989; Dingwell et al. 1996). The nature of the interactions between alumina and mafic components and boron await further experimental and spectroscopic studies.

## Applications of the experimental data

The data provided by these experiments apply to granitic liquids derived from partial melting of peraluminous protoliths at their source regions. Although the dependence of the solubility of excess alumina with

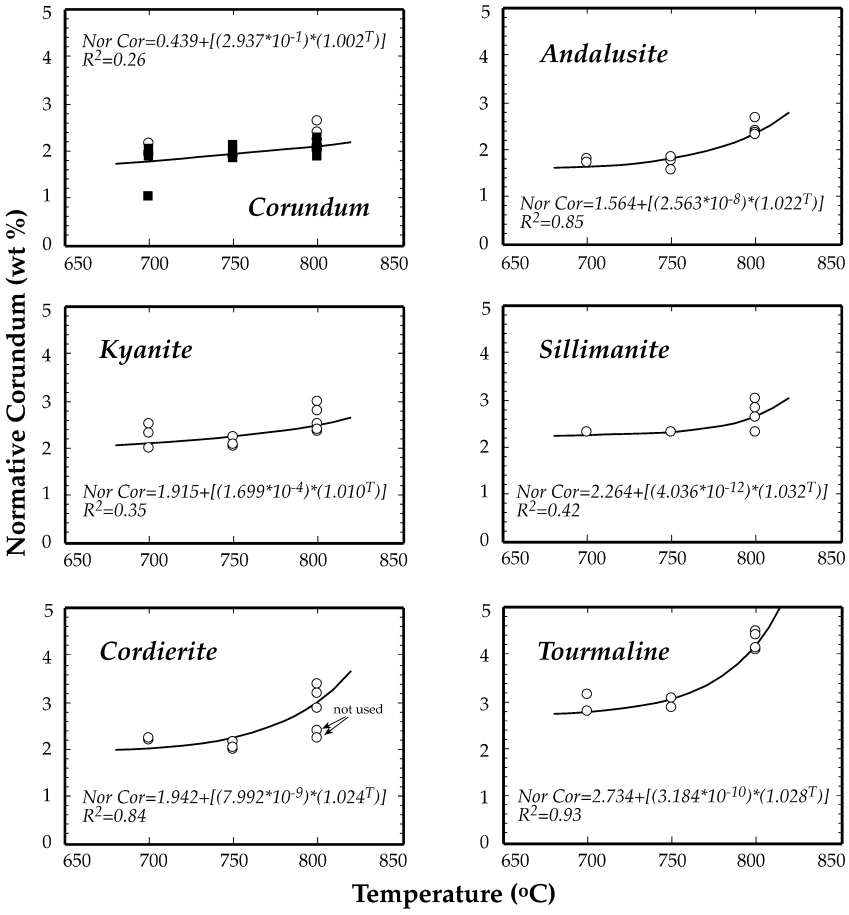


**Fig. 5** Concentration of normative corundum versus temperature for resultant experimental glasses coexisting with different peraluminous minerals

other compositional parameters like alkalis (see Patiño Douce 1992) or mafic components and B (this work) has still to be investigated in more detail, Figs. 2, 3, 4, and 5 show systematic variations that, even without additional experimentation, provide simple algorithms that relate ASI or concentration of normative corundum to temperature and $X\mathrm{H_2O}$(Melt). Based on the experimental work of Schairer and Bowen (1955, 1956), Clemens and Wall (1981), and Puziewicz and Johannes (1988), it seems reasonable to extrapolate the experimental data to slightly lower or higher $\mathrm{H_2O}$ concentrations. Due to the nature of the exponential fits, however, extrapolations to temperatures higher than 800 °C should not be made. We will discuss applications in terms of the ASI hereafter, but both ASI and normative corundum can be used given their regular variation with $T$ and $X\mathrm{H_2O}$ and the nearly perfect positive correlation between them (Fig. 7). For the purposes of modeling, it will be necessary to choose as an analogue system the ASI-$T$ and ASI-$X\mathrm{H_2O}$ relations of the most chemically complex peraluminous mineral in the system; e.g., for a typical S-type granite, we would use the solubility relations of cordierite rather than andalusite when both are present in a rock. The direct application of these data consist of using the algorithms relating ASI to temperature or $X\mathrm{H_2O}$ in order to predict theoretical values that can be compared to those observed in the natural rocks. Thus, measured ASI values lower or higher respect to those predicted might indicate or help to identify disequilibrium partial melting and melt extraction before achievement of chemical equilibrium, or the presence of restites or accumulation of early crystallized peraluminous minerals. Also, this data set can be used to infer $X\mathrm{H_2O}$ of melts when bulk composition (ASI), peraluminous mineralogy, and temperature of formation are provided. High ASI values in granitic rocks representing former melts (i.e., with very low or no restite or cumulate component) would be indicative of high $\mathrm{H_2O}$ concentrations in melt (see below). Textural information (early versus late crystallizing peraluminous phases) will provide clues about when that $X\mathrm{H_2O}$ was achieved in the history of crystallization.

## Modeling the ASI of granitic melts during anatexis

The approach followed for the modeling is as follows. Partial melting is modeled based on four different reactions (Fig. 8): (1) the wet granite solidus with muscovite present (alkali feldspar present, $\mathrm{H_2O}$ in excess), (2) the incongruent melting of muscovite with $\mathrm{H_2O}$ present (alkali feldspar absent, $\mathrm{H_2O}$ in excess), (3) fluid-absent incongruent melting of muscovite, and (4) fluid-absent incongruent melting of biotite. The temperature and

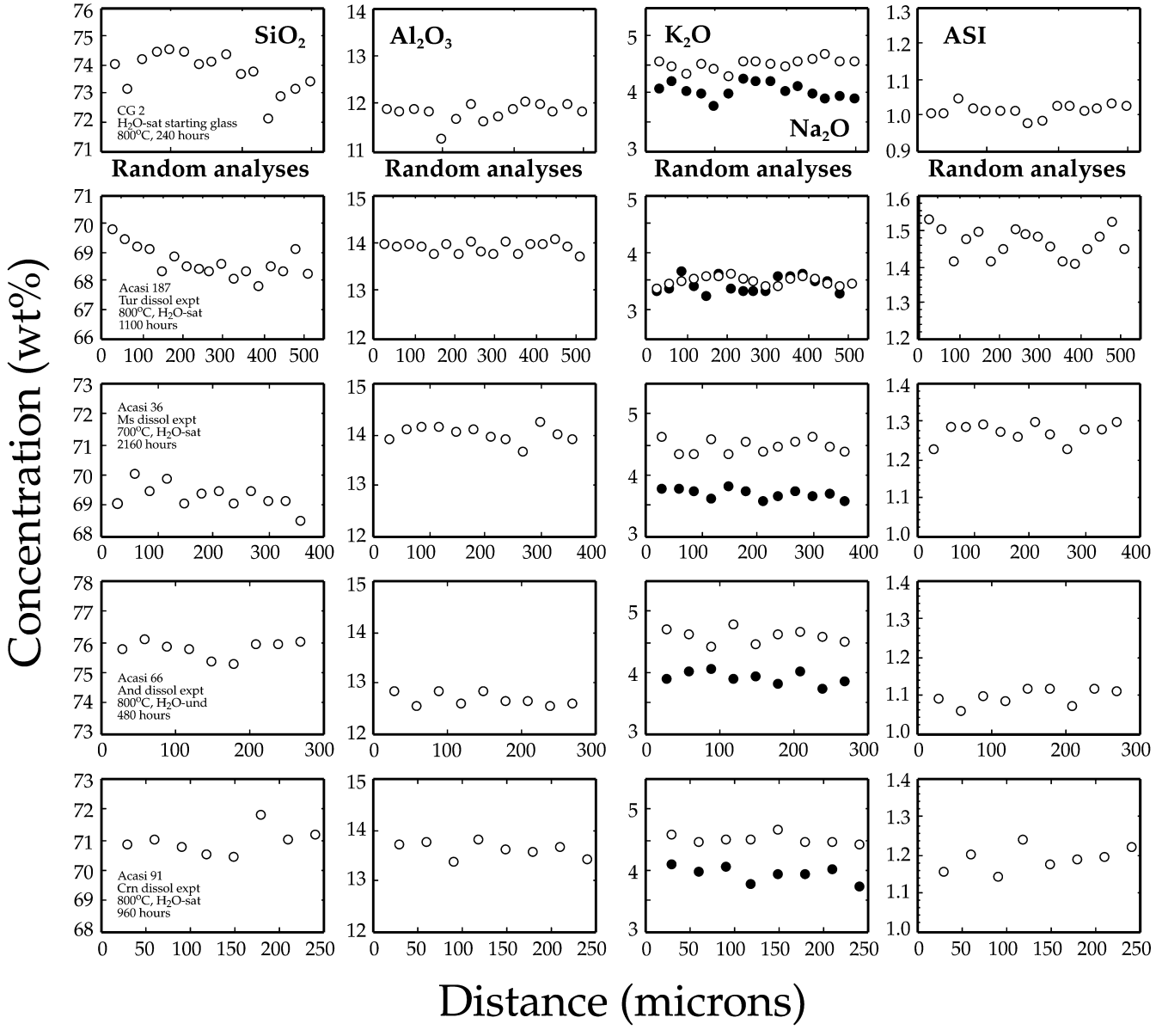


**Fig. 6** Concentration profiles in resultant experimental glass pools located between two grains of relict peraluminous minerals. Random analyses in the hydrated starting metaluminous glass are also shown for comparison. Mineral symbols after Kretz (1983)

pressure locations of these reactions are based on experimental work by Storre and Karotke (1972), Huang and Wyllie (1981), Vielzeuf and Holloway (1988), and Patiño Douce and Harris (1998). The restitic assemblage coexisting with the liquid is derived from the former authors and from chemographic relationships for high-aluminum pelites (e.g., Spear 1995). The $H_2O$ concentration of the melt during fluid-absent melting is based on the liquidus curves for the granite eutectic at different $H_2O$ concentrations (Holtz et al. 2001), and ignores the contribution of carbonaceous components derived from the oxidation of graphite. The ASI of the melt is then estimated using the regressions shown in Figs. 2 and 3, assuming equilibrium between melt and

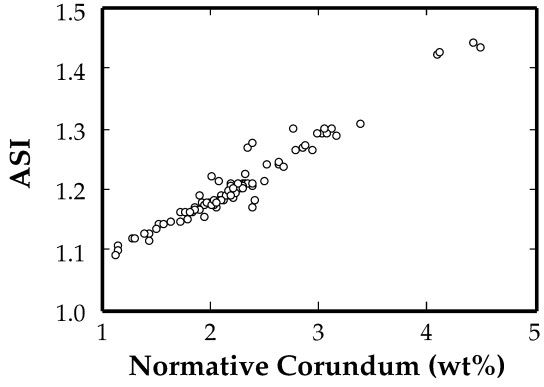


**Fig. 7** ASI versus concentration of normative corundum for all the experimental glasses

restitic assemblage. First, we calculate the ASI at the temperature of interest from Fig. 2, then this value is corrected for the $H_2O$ concentration using the slopes of

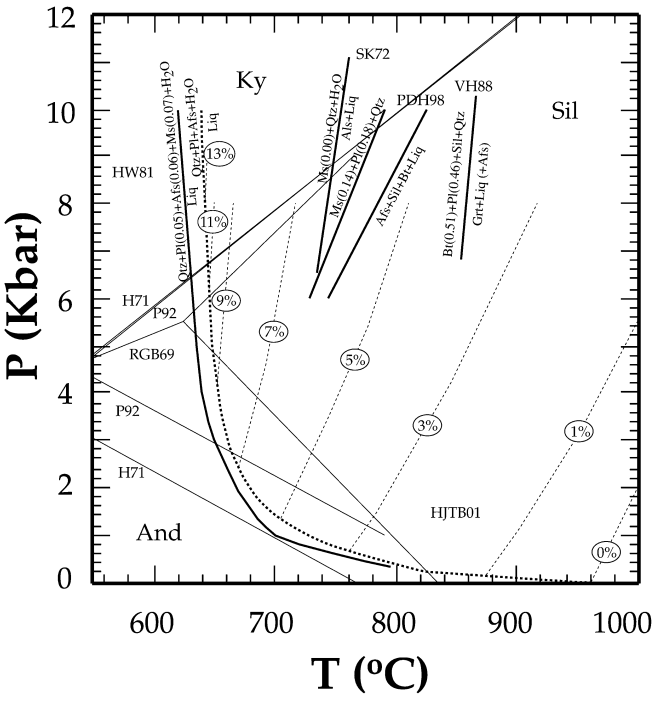


**Fig. 8** Temperature and pressure locations of some experimentally determined melting reactions for metapelites. Symbols for minerals after Kretz (1983). *Afs* Alkali feldspar, *Als* aluminum silicate, *Liq* liquid. The wet granite solidus and liquidus curves for the granite eutectic at different $H_2O$ concentrations (*dotted lines*) are taken from Holtz et al. (2001). SK72 refers to Storre and Karotke (1972), HW81 to Huang and Wyllie (1981), VH88 to Vielzeuf and Holloway (1988), PDH98 to Patiño Douce and Harris (1998), and HJTB01 to Holtz et al. (2001). *Numbers in parentheses* refer to mole fractions of anorthite component in plagioclase, albite in alkali feldspar, paragonite in muscovite, and phlogopite in biotite. Phase equilibria for the aluminum silicate polymorphs are taken from Richardson et al. (1969) (RGB69), Holdaway (1971) (H71), and Pattison (1992) (P92)

lines in Fig. 3. For instance, a liquid in equilibrium with sillimanite at 800 °C will posses an ASI of ≈1.27 at ≈7 wt% $H_2O$ in the melt (≈7 wt% is the $H_2O$ concentration at which we calculated the dependence of ASI on temperature, see Table 2), and an ASI of ≈1.17 at 3 wt% $H_2O$ in melt. In taking this approach, we make the following simplifications and assumptions: (1) the dependence of ASI on $H_2O$ concentration in melt does not vary with temperature, and is equal to that experimentally calculated at 800 °C; (2) the effect of $H_2O$ on ASI is related to $XH_2O$ rather that to $aH_2O$ (compare our results with those of Clemens and Wall (1981) and Puziewicz and Johannes (1988)); and (3) the effect of other components (Fe, Mg, B) is partially considered by choosing the ASI-$T$ and ASI-$XH_2O$ relations for the appropriate peraluminous phase. Finally, we decided not to extrapolate the experimental data at temperatures higher than 800 °C; instead minimum ASI values were calculated at 800 °C. Table 8 summarizes results of the modeling. The major conclusion is that $H_2O$-saturated melting at medium to high pressures should produce melts with distinctly greater ASI (≥ 1.30) compared to $H_2O$-undersaturated melts derived from fluid-absent incongruent melting of muscovite or biotite (≥1.20), either at low or high pressures. This is due to the critical effect of $XH_2O$ on ASI.

## Comparison with published ASI values of anatectic leucosomes and allochthonous leucogranites

When evaluated with respect to experimental and theoretical phase relationships, the mineral assemblages and thermobarometry of crustal anatectic terranes provide information about reactions, $P$–$T$ conditions, and the amount of $H_2O$ involved during partial melting. In this section we calculate experimentally predicted ASI values for specific cases of anatectic leucosomes and allochthonous leucogranites, using the mineralogy and $P$–$T$–$XH_2O$ information provided in the literature for various anatectic terranes. Comparison between measured and predicted ASI values may then supply information relevant to the extent of equilibration and to the residence time of anatectic melts with their residual peraluminous phases (e.g., Acosta-Vigil et al. 2002). This assessment aids not only the estimation of the restitic or cumulate fraction in a granitic rock, but also helps to constrain the actual proportional contributions of restitic phases to the melting assemblage in a known or potential melting reaction.

### *Anatectic leucosomes*

Leucosomes thought to approximately represent primary anatectic melts derived from aluminosilicate-rich protoliths generally possess similar or lower mean ASI values (≈1.11–1.23) compared to the experimentally predicted ones (≥1.18, Table 9). Wickham (1987) and Barbey et al. (1990) document concordant to discordant leucogranite pods with ASI values clearly lower (≈1.11–1.15) than the experimentally predicted values (≥1.20), suggesting that the granite melt was undersaturated in aluminous minerals or failed to come to equilibrium with them. In the case of the Trois Seigneurs leucogranites, Wickham (1987) pointed out that very low Zr concentrations in some samples suggest zircon-undersaturation, implying either rapid melt segregation or armoring of zircon.

Watt and Harley (1993), Barbero et al. (1995), and Bea and Montero (1999) described concordant to discordant leucosomes and tabular leucogranite bodies with mean ASI values of ≈1.17–1.23, comparable to the experimentally predicted ASI (≥ 1.18, Table 9). In detail, however, measured ASI ranges between 1.03 and 2.17 in samples from migmatites in Antarctica (Watt and Harley 1993), and between 1.03 and 1.48 in samples from migmatites in central Spain (Barbero et al. 1995). The high end of this range can be explained only by restite entrapment or accumulation of early-crystallized peraluminous phases. ASI values near the low end are most consistent with melting and liquid segregation

**Table 8** Experimentally predicted ASI values of liquids derived from partial melting of strongly peraluminous protoliths. Mineral symbols after Kretz (1983). *Afs* alkali feldspar, *Als* aluminosilicate. Al-rich mineral phases in bold refer to those used to calculate ASI values

| Melting reaction | P–T conditions | Restitic assemblage | Reference | wt% $H_2O$ in melt | ASI of melt |
|---|---|---|---|---|---|
| Qtz + Pl + Afs + Ms = liquid | 10 kb-625 to 650 °C | Qtz + Pl + **Ms** | Huang and Wyllie (1981) | > 13 | > 1.40 |
| Qtz + Pl + Afs + Ms = liquid | 6 kb-625 to 650 °C | Qtz + Pl + Afs + Crn + **Ms** | Huang and Wyllie (1981) | 11 | 1.35 |
| Ms + Qtz + $H_2O$ = Als + liquid | 10 kb-750 to 775 °C | Qtz + **Ky**/Sil + Ms + Bt ± Pl | Storre and Karotke (1972) | > 13 | > 1.55 |
| Ms + Qtz + $H_2O$ = Als + liquid | 6 kb-725 to 750 °C | Qtz + **Sil** + Ms + Bt ± Pl | Storre and Karotke (1972) | 11 | 1.32 |
| Ms + Pl + Qtz = Afs + Sil + Bt + liquid | 8 to 10 kb-750 to 825 °C | Qtz + Pl + Ms + Grt + Bt + **Sil** + Afs | Patiño Douce and Harris (1998) | 5 to 6 | 1.18–1.24 |
| Ms + Pl + Qtz = Afs + Sil + Bt + Liquid | 4 to 6 kb-700 to 750 °C | Qtz + Pl + Ms + Grt + Bt + **Sil** + Afs | Patiño Douce and Harris (1998) | 6 to 7 | 1.19–1.23 |
| Bt + Pl + Sil + Qtz = Grt + liquid (+ Afs) | 8 to 10 kb-850 to 875 °C | Qtz + **Sil** + Grt + Pl | Vielzeuf and Holloway (1988) | 4 to 5 | > 1.20 |
| Bt + Pl + Sil + Qtz = Grt + liquid (+ Crd + Afs) | 4 to 6 kb-825 to 850 °C | Qtz + **Sil** + Grt + Pl ± Crd ± Afs | Vielzeuf and Holloway (1988) | 3 to 4 | ≥1.18 |

before attainment of equilibrium with peraluminous restite, because the modeled relations of ASI-$X$$H_2O$ and ASI-$T$ for the appropriate melting conditions predict higher ASI values if crystal-melt equilibrium is attained (Table 9). These conclusions based on the ASI values are in accordance with interpretations based on petrography and the geochemistry of Zr, Th and REE in leucosomes and residual rocks (Watt and Harley 1993), and Sr isotopes and concentrations of Zr and REE in the leucogranites (Barbero et al. 1995).

These cases contrast with the narrow range in ASI values of leucosomes at Ivrea-Verbano reported by Bea and Montero (1999), between ≈1.15 and 1.22, which are close to our experimentally predicted values, ≈1.18 to 1.26 (Table 9). Also, in contrast to previous cases, Bea and Montero found that the leucosomes are saturated in zircon, monazite and apatite. Both ASI values and Zr, LREE and P geochemistry suggest, therefore, segregation of melts after equilibration with restites with respect to these components.

### *Allochthonous leucogranites*

One of the most studied granite provinces in the world is that of the Himalayan leucogranites. There are contrasting views about their origin, mainly related to fluid-present versus fluid-absent partial melting of metapelites (e.g., Le Fort 1981; Harris and Inger 1992; Inger and Harris 1993; Harris et al. 1993; Guillot and Le Fort 1995; Patiño Douce and Harris 1998). Published ASI values for the Himalayan leucogranites (Fig. 9) have a mean of ≈1.17, which compares well with our experimentally predicted ASI for the case of fluid-absent incongruent melting of muscovite (1.15–1.30, Table 9). $H_2O$-rich fluid-saturated melting of kyanite-bearing protoliths would produce strongly peraluminous melts with ASI of ≈1.40–1.50. This does not necessarily mean that partial melting took place under fluid-undersaturated conditions, because fluid-saturated partial melting with melt extraction before equilibration with aluminous restitic phases is an alternative interpretation of the data. However, if the anatectic magmas were saturated in $H_2O$, then our previous work on rates of crystal-melt equilibration (Acosta-Vigil et al. 2002) would necessitate exceedingly rapid melt extraction from restite, in less than ≈100 years, in order to prevent the attainment of crystal-liquid equilibrium.

The Harney Peak leucogranite and associated pegmatite field, South Dakota, represent one of the few large provinces of peraluminous granites in the United States. Petrogenetic studies indicate that this granite complex was formed by multiple injections of $H_2O$-undersaturated melts derived from partial melting of a compositionally heterogenous metapelitic protolith (e.g., Duke et al. 1988; Jolliff et al. 1992). The biotite-muscovite core granite crystallized from a melt derived by fluid-absent incongruent melting of biotite at ≈800–850 °C and 4.5–6 kb, whereas melts that crystallized as the peripheral muscovite-tourmaline granite and satellite

**Table 9** Measured versus experimentally predicted ASI in anatectic leucosomes and leucogranites. Mineral symbols after Kretz (1983). Al-rich mineral phases in bold refer to those used to calculate ASI values. See text for details

| Type of occurrence[a] | Locality | Reference | Melting reaction | Melting P–T conditions | Al-rich phases in restite/neosome | Assumed $H_2O$ in liquid[b] (wt%) | Mean measured ASI (No. analyses, SD) | Experimentally predicted ASI |
|---|---|---|---|---|---|---|---|---|
| B | Trois Seigneurs Massif, Pyrenees, France | Wickham (1987) | $H_2O$-saturated granite solidus | 3–4 kb, 670–700 °C | **Sil**, Crd, **Bt** | 7.5 to 9 | 1.15 (9, 0.051) | 1.21–1.25 |
| A | Yaoundé migmatites, Cameroon | Barbey et al. (1990) | Fluid-absent Bt melting | 10–12 kb, 800–850 °C | **Ky**, Grt | 6 to 6.5 | 1.11 (3, 0.055) | ≥1.23–1.26 |
| B | Brattstrand Bluffs migmatites, Antarctic Shield | Watt and Harley (1993) | Fluid-absent Bt melting | 6 kb, 860 °C | Sil, **Crd**, Grt | 3 to 3.5 | 1.23 (12,-), 1.17 (8,-) | >1.21–1.22 |
| B | Anatectic Complex of Toledo, central Spain | Barbero et al. (1995) | Fluid-absent Bt melting | 4–6 kb, 800–850 °C | Sil, **Crd**, Grt | 3 to 4.5 | 1.22 (4, 0.189) | ≥1.21–1.25 |
| A | Ivrea-Verbano, NW Italy | Bea and Montero (1999) | Fluid-absent Bt melting | 6–8 kb, 750–800 °C | **Sil**, Grt | 5 to 6 | 1.20 (4, 0.033) | 1.18–1.26 |
| C | Himalayan leucogranites | [c] | Fluid-absent Ms melting | 6–8.5 kb, 660–770 °C | Sil/**Ky** | 6 to 8, 11 to 13 | 1.17 (45, 0.085) | 1.15–1.30; 1.40–1.51 |
| C | Harney Peak leucogranites-pegmatites, South Dakota, USA | [d] | Fluid-absent Ms and Bt melting | 3.5–6 kb, 700–850 °C | **Sil** | 3 to 5, 5 to 7 | 1.17 (18, 0.065) / 1.27 (51, 0.179) | 1.17–1.23 / ≥1.17–1.22 |
| C | Lachlan Fold Belt granites, SE Australia | [e] | Fluid-absent Bt melting | 4–7 kb, 800–850 °C | **Sil**,**Crd**, Grt | 3 to 5 | 1.07–1.08, 1.10–1.14 | ≥1.17–1.22; ≥1.21–1.27 |

[a] *A* Anatectic leucosomes; *B* discordant leucogranite bodies (pods, sheets, lenses, veins and dikes) in anatectic complexes; *C* leucogranite dikes/plutons intruding rocks structurally above the anatectic complex

[b] Calculated based on minimum $H_2O$ concentrations given by Holtz et al. (2001) and P–T conditions given by the source authors.

[c] Le Fort (1981), Searle and Fryer (1986), Stern et al. (1989), Scaillet et al. (1990), Inger and Harris (1993), Guillot and Le Fort (1995), Searle et al. (1997).

[d] Rockhold et al. (1987), Duke et al. (1992), Nabelek et al. (1992).

[e] Clemens and Wall (1981), Chappell et al. (1987).

intrusions formed by fluid-absent incongruent melting of muscovite at ≈700–750 °C and 3.5–5 kb (Nabelek et al. 1992; Shearer et al. 1992; Nabelek and Glascok 1995). The mean ASI values of central and peripheral granites, ≈1.17 and ≈1.27, respectively (Fig. 9), (Rockhold et al. 1987; Duke et al. 1992; Nabelek et al. 1992), are within the range of experimentally predicted values for the specified conditions, 1.17–1.23 and ≥1.17–1.22, respectively (Table 9). Our results, therefore, are in accord with these conclusions.

Granites of the Lachlan Fold Belt in southeastern Australia have formed the basis for one of the mostly widely used schemes for the classification of granite according to source material (I- versus S-type: White and Chappell 1977). Two contrasting models for chemical variation among granite suites include restite unmixing (White and Chappell 1977; Chappell et al. 1987; Chappell 1996) and magma mixing (Collins 1996; Keay et al. 1997). The parental melts for some of the peraluminous S-type rhyolites (Violet Town Volcanics) were inferred to originate at 800–850 °C, 4–7 kb, with $H_2O$ concentrations of 3–5 wt% (Clemens and Wall 1981). Chappell et al. (1987) suggested temperatures of 800 °C or a little less than 800 °C, moderate pressures, and fluid-undersaturated conditions for the generation of the parental melts of the Bullenbalong supersuite and Violet Town Volcanics. At these conditions, our experiments predict an ASI of ≥1.17–1.22 and ≥1.21–1.27 for melts coexisting with sillimanite or cordierite, respectively (Table 9). The ASI values of the Australian S-type rocks that are considered to represent unfractionated and restite-free parental melts are lower, e.g., 1.10–1.14 (Clemens and Wall 1984) or 1.07–1.08 (Chappell et al. 1991; Chappell 1999). Clemens and Wall (1981, 1984) attributed these low ASI values to weakly to mildly peraluminous metasedimentary magma sources, implying that the magmas contained a large metaluminous component. Most S-types, however, contain cordierite and are thought to be derived from cordierite-bearing sources (e.g., Chappell et al. 1987); this means that they have been saturated with respect to cordierite from their inception. For example, the Numbla Vale Adamellite, which is regarded by Chappell et al. (1991) as an unfractionated $H_2O$-undersaturated and restite-free "minimum-temperature S-type melt", contains cordierite but possesses a whole-rock ASI of only 1.08. This is in general accordance with our experimental results showing that low $H_2O$ concentrations in melt promote lower ASI values. An alternative explanation, therefore, points to very low $H_2O$ contents in the melt, lower even than indicated by our model reactions involving fluid-absent incongruent melting of micas. Other explanations involve magma mixing between crustal and mantle components (Collins 1996; Elburg 1996; Keay et al. 1997), or that these rocks crystallized from magmas resulting from low-pressure interaction of basaltic melts with Al-rich metasediments, and incorporated solid phases (plagioclase and orthopyroxene) produced during the interaction (Patiño Douce 1999).

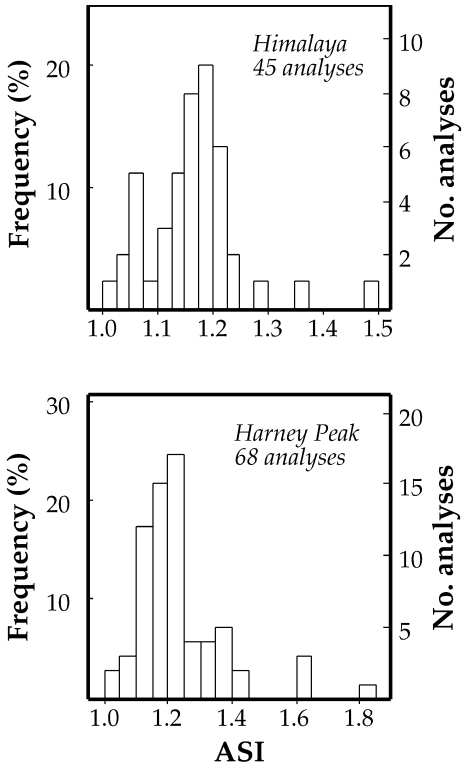


**Fig. 9** Frequency of ASI values in the Himalayan leucogranites (data from Le Fort 1981; Searle and Fryer 1986; Stern et al. 1989; Scaillet et al. 1990; Inger and Harris 1993; Guillot and Le Fort 1995; Searle et al. 1997) and the Harney Peak leucogranites (Rockhold et al. 1987; Duke et al. 1992; Nabelek et al. 1992)

## Conclusions

The principal conclusion from this work is that the ASI values and concentrations of normative corundum of granitic liquids derived from the partial melting of peraluminous protoliths vary in regular and predictable ways as functions of $T$-$X\mathrm{H_2O}$ conditions during anatexis, which control the composition of the melt and the mineral assemblage in the restite. The primary controls on ASI and normative corundum of melt are the availability of $H_2O$, the temperature, and the contributions of non-haplogranite components via the relevant melting reactions. In this paper, we have experimentally derived a set of relations to predict the melt ASI and normative corundum, appropriate for melt compositions of increasing chemical complexity as reflected by the sequence corundum, aluminosilicates, cordierite, and tourmaline. The choice of appropriate buffering reactions can be made from modal analysis or normative analysis of the whole rocks. With these constraints, we have used this data set to predict ASI values for a series of anatectic leucosomes and allochthonous leucogranites whose compositions and $P$–$T$–$X\mathrm{H_2O}$ of formation have been reported in the literature. In a few cases, the low ASI of some of these natural rocks (in comparison to experimentally predicted values) might be attributed to rapid extraction of melt from restite before the attainment of crystal-melt equilibrium (e.g., Acosta-Vigil et al. 2002). In most instances, however, the low to moderate ASI values of allochthonous granites can be explained by low $H_2O$ concentrations in melt (e.g., due to partial melting by fluid-absent incongruent melting of micas) and relatively unfractionated, restite-free magmas. These interpretations are consistent with the results of prior petrologic studies on these rocks. We can further suggest that the ASI of peraluminous leucogranite magmas should increase with crystal fractionation, as suggested by Chappell (1999), to higher values as melts approach saturation in $H_2O$. Combined with kinetic studies on the dissolution of peraluminous minerals (Acosta-Vigil et al. 2002), and together with other petrological and geochemical tools already available (e.g., kinetic studies on zircon, monazite and apatite dissolution, kinetic studies on Sr and Nd isotopic equilibration), ASI values and concentrations of normative corundum may provide information about melt generation and segregation time frames, presence of restites/early crystallized peraluminous phases, and $H_2O$-absent versus $H_2O$-present partial melting in the continental crust. Future work should refine the dependence of ASI with $T$ (especially at temperatures higher than 800 °C), with $H_2O$ concentration (especially at very low or high concentrations), and the effect of $H_2O$ on ASI at temperatures other than 800 °C.

**Acknowledgements** Support for this research was provided by National Science Foundation grants EAR-990165, INT-9603199, EAR-9618867, EAR-9625517, and EAR-9404658, and a postdoctoral grant to AAV from the Universidad de Granada, Spain. Detailed reviews by Dana Johnston and Alberto Patiño Douce improved an earlier version of the manuscript and are very much appreciated.

## References

Acosta-Vigil A, London D, Dewers TA, Morgan VI GB (2002) Dissolution of corundum and andalusite in $H_2O$-saturated haplogranitic melts at 800 °C and 200 MPa: constraints on diffusivities and the generation of peraluminous melts. J Petrol 43:1885–1908

Ayres M, Harris N, Vance D (1997) Possible constraints on anatectic melt residence times from accessory mineral dissolution rates: an example from Himalayan leucogranites. Min Mag 61:29–36

Barbero L, Villaseca C, Rogers G, Brown PE (1995) Geochemical and isotopic disequilibrium in crustal melting: an insight from the anatectic granitoids from Toledo, Spain. J Geophys Res 100:15745–15765

Barbey P, Macaudiere J, Nzenti JP (1990) High-pressure dehydration melting of metapelites: evidence from the Migmatites of Yaoundé (Cameroon). J Petrol 31:401–427

Bea F, Montero P (1999) Behaviour of accessory phases and redistribution of Zr, REE, Y, Th, and U during metamorphism and partial melting of metapelites in the lower crust: an example from the Kinzigite Formation of Ivrea-Verbano, NW Italy. Geochim Cosmochim Acta 63:1133–1153

Behrens H, Jantos N (2001) The effect of anhydrous composition on water solubility in granitic melts. Am Mineral 86:14–20

Chappell BW (1996) Magma mixing and the production of compositional variation within granite suites: evidence from the granites of southeastern Australia. J Petrol 37:449–470
Chappell BW (1999) Aluminum saturation in I- and S-type granites and the characterization of fractionated haplogranites. Lithos 46:535–551
Chappell BW, White AJR (1974) Two contrasting granite types. Pac Geol 8:173–174
Chappell BW, White AJR, Williams IS (1991) A transverse section through granites of the Lachlan Fold Belt. Second Hutton Symposium excursion guide. Bureau of Mineral Resources, Geology and Geophysics, Record 1991/22
Chappell BW, White AJR, Wyborn D (1987) The importance of residual source material (restite) in granite petrogenesis. J Petrol 28:1111–1138
Clemens JD, Wall VJ (1981) Origin and crystallization of some peraluminous (S-type) granitic magmas. Can Mineral 19:111–131
Clemens JD, Wall VJ (1984) Origin and evolution of a peraluminous silicic ignimbrite suite: the violet town volcanics. Contrib Mineral Petrol 88:354–371
Collins WJ (1996) Lachlan Fold Belt granitoids: products of three-component mixing. Trans R Soc Edinb: Earth Sci 87:171–181
Copeland P, Harrison TM, Le Fort P (1990) Age and cooling history of the Manaslu granite: implications for Himalayan tectonics. J Volcanol Geotherm Res 44:33–50
Dickenson MP, Hess PC (1981) Redox equilibria and the structural role of iron in alumino-silicate melts. Contrib Mineral Petrol 78:352–357
Dingwell DB, Harris DM, Scarfe CM (1984) The solubility of $H_2O$ in melts in the system $SiO_2$-$Al_2O_3$-$Na_2O$-$K_2O$ at 1 to 2 kbars. J Geol 92:387–395
Dingwell DB, Holtz F, Behrens H (1997) The solubility of $H_2O$ in peralkaline and peraluminous granitic melts. Am Mineral 82:434–437
Dingwell DB, Pichavant M, Holtz F (1996) Experimental studies of boron in granitic melts. In: Grew ES, Anovitz LM (eds) Boron: mineralogy, petrology and geochemistry. Mineral Soc Am, Rev Mineral 33:331–385
Duke EF, Papike JJ, Laul JC (1992) Geochemistry of a boron-rich peraluminous granite pluton: the Calamity Peak layered granite-pegmatite complex, Black Hills, South Dakota. Can Mineral 30:811–833
Duke EF, Redden JA, Papike JJ (1988) Calamity Peak layered granite-pegmatite complex, Black Hills, South Dakota. 1. Structure and emplacement. Geol Soc Am Bull 100:1244–1259
Elburg MA (1996) Genetic significance of multiple enclave types in a peraluminous ignimbrite suite, Lachlan Fold Belt, Australia. J Petrol 37:1385–1408
Guillot S, Le Fort P (1995) Geochemical constraints on the bimodal origin of High Himalayan leucogranites. Lithos 35:221–234
Gwinn R, Hess PC (1989) Iron and titanium solution properties in peraluminous and peralkaline rhyolitic liquids. Contrib Mineral Petrol 101:326–338
Harlov DE, Milke R (2002) Stability of corundum + quartz relative to kyanite and sillimanite at high temperature and pressure. Am Mineral 87:424–432
Harris NBW, Inger S (1992) Trace element modelling of pelite-derived granites. Contrib Mineral Petrol 110:46–56
Harris N, Inger S, Massey J (1993) The role of fluids in the formation of High Himalayan leucogranites. In: Treloar PJ, Searle MP (eds) Himalayan tectonics. Geol Soc Spec Publ 74:391–400
Harris N, Vance D, Ayres M (2000) From sediment to granite: timescales of anatexis in the upper crust. Chem Geol 162:155–167
Holdaway MJ (1971) Stability of andalusite and the aluminum silicate phase diagram. Am J Sci 271:97–131
Holtz F, Johannes W, Pichavant M (1992a) Peraluminous granites: the effect of alumina on melt composition and coexisting minerals. Trans R Soc Edinb: Earth Sci 83:409–416
Holtz F, Johannes W, Pichavant M (1992b) Effect of excess aluminum on phase relations in the system Qz-Ab-Or. Experimental investigation at 2 kbar and reduced $H_2O$ activity. Eur J Mineral 4:137–152
Holtz F, Behrens H, Dingwell DB, Johannes W (1995) $H_2O$ solubility in haplogranitic melts: compositional, pressure, and temperature dependence. Am Mineral 80:94–108
Holtz F, Behrens H, Dingwell DB, Taylor RP (1992c) Water solubility in aluminosilicate melts of haplogranite composition at 2 kbar. Chem Geol 96:289–302
Holtz F, Johannes W, Tamic N, Behrens H (2001) Maximum and minimum water contents of granitic melts generated in the crust: a reevaluation and implications. Lithos 56:1–14
Huang WL, Wyllie PJ (1981) Phase relationships of S-type granite with $H_2O$ to 35 kbar: muscovite granite from Harney Peak, South Dakota. J Geophys Res 86:10515–10529
Inger S, Harris NBW (1993) Geochemical constraints on leucogranite magmatism in the Langtang Valley, Nepal Himalaya. J Petrol 34:345–368
Jolliff BL, Papike JJ, Shearer CK (1992) Petrogenetic relationships between pegmatite and granite based on geochemistry of muscovite in wall zones, Black Hills, South Dakota, USA. Geochim Cosmochim Acta 56:1915–1939
Joyce DB, Voigt DE (1994) A phase equilibrium study in the system $KAlSi_3O_8$- $NaAlSi_3O_8$-$SiO_2$-$Al_2SiO_5$-$H_2O$ and petrogenetic implications. Am Mineral 79:504–512
Keay S, Collins WJ, McCulloch MT (1997) A three-component Sr-Nd isotopic mixing model for granitoid genesis, Lachlan Fold Belt, eastern Australia. Geology 25:307–310
Kretz R (1983) Symbols for rock-forming minerals. Am Mineral 68:277–279
Lacy ED (1963) Aluminum in glasses and melts. Phys Chem Glasses 4:234–238
Le Fort P (1981) Manaslu leucogranite: a collision signature of the Himalaya. A model for its genesis and emplacement. J Geophys Res 86:10545–10568
Linnen RL, Pichavant M, Holtz F (1996) The combined effects of $fO_2$ and melt composition on $SnO_2$ solubility and tin diffusivity in haplogranitic melts. Geochim Cosmochim Acta 60: 4965–4976
Linnen RL, Pichavant M, Holtz F, Burgess S (1995) The effects of $fO_2$ on the solubility, diffusion, and speciation of tin in haplogranitic melts at 850 °C and 2 kbar. Geochim Cosmochim Acta 59:1579–1588
London D, Morgan VI GB, Babb HA, Loomis JL (1993) Behaviour and effects of phosphorus in the system $Na_2O$–$K_2O$–$Al_2O_3$–$Si_2O$–$P_2O_5$-$H_2O$ at 200 MPa $H_2O$. Contrib Mineral Petrol 114:450–465
Morgan VI GB, London D (1996) Optimizing the electron microprobe analysis of hydrous alkali aluminosilicate glasses. Am Mineral 81:1176–1185
Mungall JE, Romano C, Dingwell DB (1998) Multicomponent diffusion in the molten system $K_2O$-$Na_2O$-$Al_2O_3$-$SiO_2$-$H_2O$. Am Mineral 83:685–699
Mysen BO (1987) Redox equilibria and coordination of $Fe^{2+}$ and $Fe^{3+}$ in silicate glasses from $^{57}Fe$ Mossbauer spectroscopy. J Non-Cryst Solids 95–96:247–254
Mysen BO, Virgo D, Kushiro I (1981) The structural role of aluminum in silicate melts—a Raman spectroscopic study at 1 atmosphere. Am Mineral 66:678–701
Mysen BO, Virgo D, Newman E-R, Siefert FA (1985) Redox equilibria and the structural states of ferric and ferrous iron in melts in the system CaO-MgO-$Al_2O_3$-$SiO_2$-Fe-O: relationships between redox equilibria, melt structure and liquidus phase equilibria. Am Mineral 70:317–331
Nabelek PI, Glascock MD (1995) REE-depleted leucogranites, Black Hills, South Dakota: a consequence of disequilibrium melting of monazite-bearing schists. J Petrol 36:1055–1071
Nabelek PI, Russ-Nabelek C, Denison JR (1992) The generation and crystallization conditions of the Proterozoic Harney Peak Leucogranite, Black Hills, South Dakota, USA: petrologic and geochemical constraints. Contrib Mineral Petrol 110: 173–191
Patiño Douce AE (1992) Calculated relationships between activity of alumina and phase assemblages of silica-saturated igneous rocks. J Volcanol Geotherm Res 52:43–63

Patiño Douce AE (1999) What do experiments tell us about the relative contributions of crust and mantle to the origin of granitic magmas? In: Castro A, Fernández C, Vigneresse JL (eds) Understanding granites: integrating new and classical techniques. Geological Society, London, Special Publications 168, pp 55–75

Patiño Douce AE, Harris N (1998) Experimental constraints on Himalayan anatexis. J Petrol 39:689–710

Pattison DRM (1992) Stability of andalusite and sillimanite and the $Al_2SiO_5$ triple point, constraints from the Ballachulish aureole, Scotland. J Geol 100:423–446

Pereira MD, Bea F (1994) Cordierite-producing reactions at the Peña Negra complex, Avila batholith, central Spain: the key role of cordierite in low-pressure anatexis. Can Mineral 32:763–780

Poe BT, McMillan PF, Coté B, Massiot D, Coutures JP (1992) $SiO_2$-$Al_2O_3$ liquids: in situ study by high temperature $^{27}Al$ NMR spectroscopy and molecular dynamics simulations. J Phys Chem 96:8220–8224

Pouchou JL, Pichoir F (1985) $\rho(\varphi z)$ correction procedure for improved quantitative microanalysis. In: Armstrong JT (ed) Microbeam analysis. San Francisco Press, San Francisco, pp 104–106

Puziewicz J, Johannes W (1988) Phase equilibria and compositions of Fe-Mg-Al minerals and melts in water-saturated peraluminous granitic systems. Contrib Mineral Petrol 100:156–168

Richardson SW, Gilbert MC, Bell PM (1969) Experimental determination of kyanite-andalusite and andalusite-sillimanite equilibria: the aluminum silicate triple point. Am J Sci 267:259–272

Rockhold JR, Nabelek PI, Glascock MD (1987) Origin of rhythmic layering in the Calamity Peak satellite pluton of the Harney Peak Granite, South Dakota: the role of boron. Geochim Cosmochim Acta 51:487–496

Sato RK, McMillan PF, Dennison P, Dupree R (1991) A structural investigation of high alumina content glasses in the CaO-$Al_2O_3$-$SiO_2$ system via Raman and MAS NMR. Phys Chem Glasses 32:149–154

Sawyer EW (1991) Disequilibrium melting and the rate of melt separation during migmatization of mafic rocks from the Grenville Front, Quebec. J Petrol 32:701–738

Scaillet B, France-Lanord C, Le Fort P (1990) Badrinath-Gangotri plutons (Garhwal, India): petrological and geochemical evidence for fractionation processes in a high Himalayan leucogranite. J Volcanol Geotherm Res 44:163–188

Schairer JF, Bowen NL (1955) The system $K_2O$–$Al_2O_3$–$SiO_2$. Am J Sci 253:681–746

Schairer JF, Bowen NL (1956) The system $Na_2O$–$Al_2O_3$–$SiO_2$. Am J Sci 254:129–195

Searle MP, Fryer BJ (1986) Garnet, tourmaline and muscovite-bearing leucogranites, gneisses and migmatites of the higher Himalayas from Zanskar, Kulu, Lahoul and Kashmir. In: Coward MP, Ries AC (eds) Collision tectonics. Geol Soc Spec Publ 19:185–201

Searle MP, Parrish RR, Hodges KV, Hurford A, Ayres MW, Whitehouse MJ (1997) Shisha Pangma leucogranite, South Tibetan Himalaya: field relations, geochemistry, age, origin, and emplacement. J Geol 105:295–317

Shearer CK, Papike JJ, Jolliff BL (1992) Petrogenetic links among granites and pegmatites in the Harney Peak rare-element granite-pegmatite system, Black Hills, South Dakota. Can Mineral 30:785–809

Silver L, Stolper E (1989) Water in albitic glasses. J Petrol 30:667–709

Spear FS (1995) Metamorphic phase equilibria and pressure–temperature-time paths. Mineralogical Society of America Monograph, BookCrafters Inc, Chelsea, Michigan

Stern CR, Kligfield R, Schelling D, Virdi NS, Futa K, Peterman ZE, Amini H (1989) The Bhagirathi leucogranite of the high Himalaya (Garhwal, India); age, petrogenesis, and tectonic implications. Geol Soc Am Spec Pap 232:33–45

Storre B, Karotke E (1972) Experimental data on melting reactions of muscovite + quartz in the system $K_2O$–$Al_2O_3$–$SiO_2$–$H_2O$ to 20 kb water pressure. Contrib Mineral Petrol 36:343–345

Taylor JR, Wall VJ (1992) The behaviour of tin in granitoid magmas. Econ Geol 87:403–420

Tuttle OF, Bowen NL (1958) Origin of granite in the light of experimental studies in the system $NaAlSi_3O_8$–$KAlSi_3O_8$–$SiO_2$–$H_2O$. Geol Soc Am Mem 74

Vielzeuf D, Holloway JR (1988) Experimental determination of the fluid-absent melting relations in the pelitic system. Contrib Mineral Petrol 98:257–276

Virgo D, Mysen BO (1985) The structural state of iron in oxidized vs. reduced glasses at 1 atm; a $^{57}Fe$ Moessbauer study. Physics and chemistry of minerals 12. Springer, Berlin Heidelberg New York, pp 65–76

Watt GR, Harley SL (1993) Accessory phase controls on the geochemistry of crustal melts and restites produced during water-undersaturated partial melting. Contrib Mineral Petrol 114:550–566

Watt GR, Burns IM, Graham GA (1996) Chemical characteristics of migmatites: accessory phase distribution and evidence for fast melt segregation rates. Contrib Mineral Petrol 125: 100–111

Weill DF (1966) Stability relations in the $Al_2O_3$-$SiO_2$ system calculated from solubilities in the $Al_2O_3$–$SiO_2$–$Na_3AlF_6$ system. Geochim Cosmochim Acta 30:223–237

White AJR, Chappell BW (1977) Ultrametamorphism and granitoid genesis. Tectonophysics 43:7-22

Wickham SM (1987) Crustal anatexis and granite petrogenesis during low-pressure regional metamorphism: the Trois Seigneurs Massif, Pyrenees, France. J Petrol 28:127–169

Wolf BM, London D (1997) Boron in granitic magmas: stability of tourmaline in equilibrium with biotite and cordierite. Contrib Mineral Petrol 130:12–30

Zen E (1986) Aluminum enrichment in silicate melt by fractional crystallization: some mineralogic and petrographic constraints. J Petrol 27:1095–1117